Available online at www.sciencedirect.com
ScienceDirect
Journal of Sound and Vibration 304 (2007) 691–721
JOURNAL OF SOUND AND VIBRATION
www.elsevier.com/locate/jsvi

Wave propagation in light weight profiles with truss-like cores: Wavenumber content, forced response and influence of periodicity perturbations

Torsten Kohrs*, Björn A.T. Petersson

Institute of Fluid Mechanics and Engineering Acoustics, Technical University of Berlin, Einsteinufer 25, 10587 Berlin, Germany

Received 31 October 2006; received in revised form 22 February 2007; accepted 6 March 2007

Abstract

The wavenumber content of periodic light weight profile strips is investigated. Theory of wave propagation in multi-coupled periodic systems is used to extract the dispersion characteristics of typical configurations. Solving the transfer matrix eigenvalue problem forms a basis for understanding the wave propagation in (infinite) strips; six characteristic waves travelling in each direction occur, either propagating, decaying or complex. Each characteristic wave consists of multiple wavenumbers of different amplitude, forming the so called "space harmonic" series. Typical wave forms of characteristic waves are shown and form the basis for identifying their relative contributions in the space harmonic series.

Based on the dynamic stiffness matrix of a single subelement of the periodic system the forced response is calculated for infinite light weight profile strips. The characteristic wave amplitudes for selected force excitations in combination with the corresponding wavenumber spectra form the basis for structural acoustic investigations. Input mobilities for the infinite strip are presented demonstrating the typical pass and stop band behaviour. A brief study of the influence of periodicity perturbations reveals that for typical profiles, even quite high random length variations up to about 10% have a limited effect on the structural dynamics of the strip.

1. Introduction

Light weight profiles exemplified in Fig. 1 are used in several industrial applications, e.g. for train carriages. The study focusses on the wave propagation in such structures, which comprise a high static stiffness in combination with low mass. Often there are two thin outer plates connected via inclined or perpendicular stiffeners.

Most of the profiles are periodic or nearly periodic and typical effects like pass and stop band behaviour are expected. Periodic structures have been investigated intensively in the last decades, e.g. Refs. [1–3].

Different approaches to describe the structural–acoustic characteristics of light weight profiles can be found in literature. The global behaviour of the profile, dominating in the low-frequency regime, is investigated using

*Corresponding author. Tel.: +49 30 314 22203; fax: +49 30 314 25135.
E-mail address: torsten.kohrs@tu-berlin.de (T. Kohrs).

0022-460X/$ - see front matter © 2007 Elsevier Ltd. All rights reserved.
doi:10.1016/j.jsv.2007.03.022

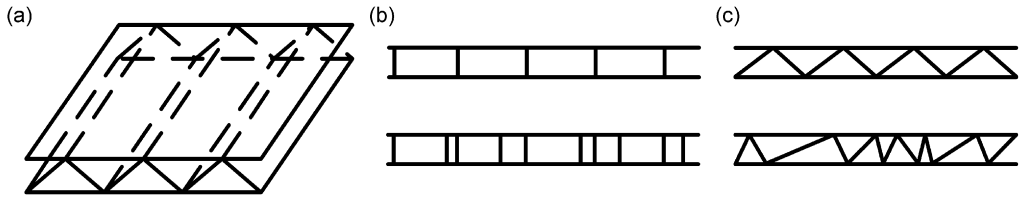

Fig. 1. (a) Periodic light weight plate; (b) cross sections with vertical webs; (c) cross sections with inclined webs.

a sandwich approach by Lok and Cheng [4,5]. The structure is treated as an equivalent orthotropic plate. For higher frequencies, where local vibrations of the structural members appear, different approaches are necessary. Statistical methods are applied by Geissler and Neumann [6] and Xie et al. [7]. Xie et al. demonstrate that for a typical railway carriage profile the local vibrations dominate at frequencies above 300 Hz.

Pezerat and Guyader [8] use an analytical modal approach to describe the structural acoustic characteristics of light weight profiles, whereas El-Raheb [9] uses a transfer matrix approach. Pezerat and Guyader focus on the eigenmodes and the transmission loss, whereas El-Raheb concentrates on the influence of different parameters (curvature, mass, damping) on the mean structural response of a two-dimensional strip.

Signorelli and von Flotow [10] investigate the wave propagation in periodic truss beams in detail. Characteristic waves are extracted and the periodic system effects are investigated. As only the translational degrees of freedom at the joints are included, results are strictly valid only for the special case of suppressed rotations at the joints. Emaci et al. [11] deal with truss structures of similar shapes and identify the characteristic waves for the periodic system. In the first part, they use the complete formulation including rotational components at the joints. No detailed investigation of the wavenumber content is included so that the results are not applicable for sound radiation phenomena, which is indeed not intended for the investigated structures there. Ruzzene [12] investigates the dynamics and sound radiation of sandwich beams with honeycomb truss core and also with a 'square' core, similar to one of the geometries investigated here. The calculation is based on the spectral finite element method and results are presented for finite strip configurations. No use is made of periodic system theory and the wave propagation is not investigated. Sound radiation is treated and a comparison with a unit cell analysis with special guided boundary condition agree principally with the results for the complete strip, at least for the investigated average response for normally incident pressure wave excitation.

Often the lightweight structures are periodic or nearly periodic. This is especially true for industrial standard profiles, designed for a variety of applications. The details of the structural loads are unknown or locally varying and hence no specific (static) design is performed, reinforcing for example the load carrying regions. Periodic structures show some characteristic effects which have been studied extensively in the past (cf. e.g. Refs. [13,1–3]). The periodic nature simplifies the calculation procedure as only one periodic subsystem has to be analysed. The wave propagation of a complete (infinite) profile strip can be deduced from the subsystem results.

The most important feature of the wave propagation in periodic structures is the existence of pass- and stop-bands, where unhindered and strongly suppressed wave propagation occurs, respectively. Hence, the wave propagation undergoes a mechanical bandpass filtering [14].

A general theory for the wave propagation in mono- and multi-coupled structural periodic systems has been developed by Mead [1,2]. Mono-coupled periodic systems are connected by only one displacement variable in contrast to multi-coupled systems. The light weight profiles investigated here are typical members of the multi-coupled case for which a general theory is thoroughly presented in Ref. [15].

In this study an analytical approach is chosen to investigate the wave propagation in the light weight structures. The calculation model based on analytical beam functions for bending and longitudinal vibrations is established in Ref. [16]. Three different strip geometries are investigated. The resulting mobilities for these periodic finite systems show typical pass and stop band behaviour.

In order to get a better understanding of the structure-borne sound characteristics of typical light weight profiles, the wave propagation in sample strips is investigated. The objective is to identify the characteristic

waves that propagate or decay in the strips. The wavenumber content of the outer plates forms the basis for treating sound radiation problems. Based on the calculation model established and validated in Ref. [16], the wavenumber content and wave forms of the characteristic waves in the infinite light weight structures is investigated.

The wave amplitudes of the characteristic waves are studied for forced excitation of infinite strips. Moreover, the influence of structural periodicity perturbations on the behaviour of the strip is discussed briefly, as in reality no strict periodicity can be achieved, e.g. because of manufacturing tolerances.

2. Dispersion characteristics of profile strips

Three profiles A–C comprising different truss-like core geometries are introduced in Ref. [16] with full physical properties. The calculation of the strip dynamics is based on analytical beam functions including both bending and longitudinal vibrations. A detailed description can be found in Ref. [16]. The geometries of the three profile strips A–C are visualized with their characteristic wave forms in Figs. 10–12.

For the profiles A–C the wavenumber content of the characteristic waves is investigated using three different methods. The first one uses the determinantal equation resulting from multi-coupled periodic system theory. The complete set of procedures is illustrated in Fig. 2. In order to catch the wave propagation in the profile strips without the influence of end reflections, the calculation is performed on prolonged strips or based on infinite strip theory.

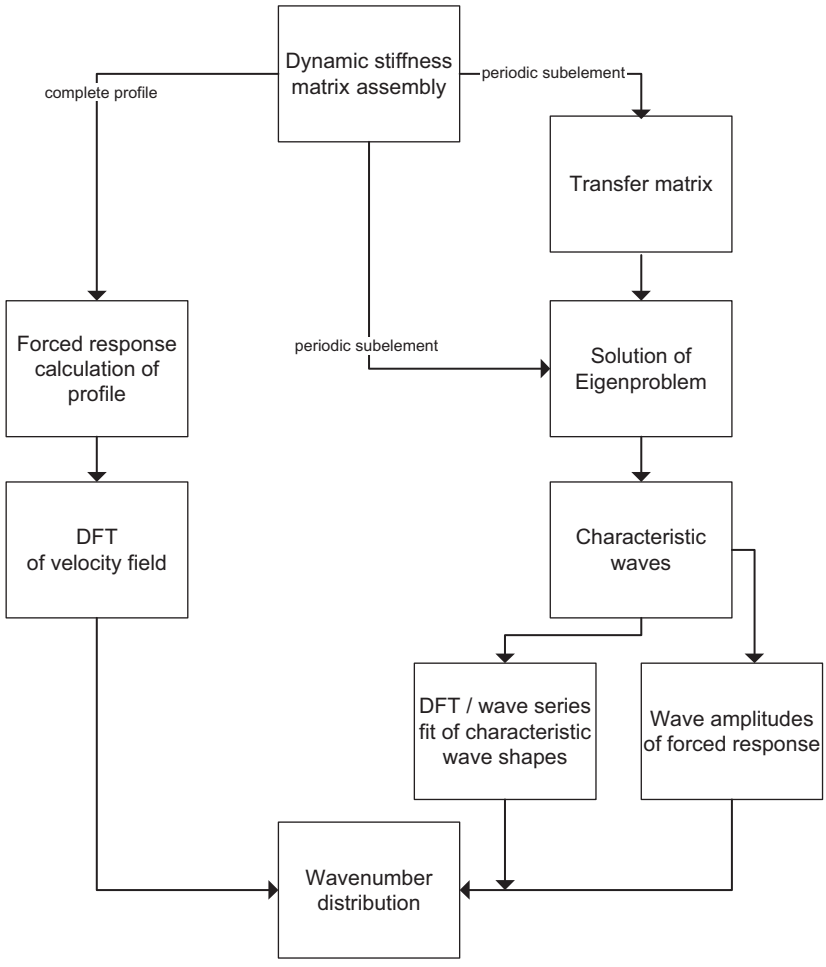

Fig. 2. Principal ways to determine dispersion characteristics (quantitative wavenumber distribution) of profile strip.

2.1. Multi-coupled periodic systems and determinantal equation

The subsystems of the light weight profile strips under study are connected at two points with three degrees of freedom each, resulting in a multi-coupled periodic system with six coupling coordinates. No detailed review of the theory for multi-coupled periodic systems will be given, but some main features shall be highlighted.

A single subsystem of the periodic system is coupled to the adjacent subsystems by n_{dof} degrees of freedom (dofs), which can be arbitrarily translational or rotational dofs. Hence, the mobility matrix of a subsystem including the left and right connection points can be formulated using a $(2n_{\mathrm{dof}}) \times (2n_{\mathrm{dof}})$ mobility matrix $\mathbf{Y}$:

$$\begin{Bmatrix} \mathbf{v_l} \\ \mathbf{v_r} \end{Bmatrix} = \mathbf{Y} \begin{Bmatrix} \mathbf{F_l} \\ \mathbf{F_r} \end{Bmatrix} = \begin{bmatrix} \mathbf{Y_{ll}} & \mathbf{Y_{lr}} \\ \mathbf{Y_{rl}} & \mathbf{Y_{rr}} \end{bmatrix} \begin{Bmatrix} \mathbf{F_l} \\ \mathbf{F_r} \end{Bmatrix}. \tag{1}$$

Here, index l represents quantities on the left-hand side of the element and index r represents the quantities on the right. The vectors $\mathbf{v}$ and $\mathbf{F}$ may contain translational and rotational quantities.

Assuming now that the quantities on the left are always related to the quantities on the right by an exponential factor (Bloch's theorem), one may write the following relation using the complex propagation constant $\mu = -\delta \pm \mathrm{j}\varepsilon$:

$$\begin{aligned} \{\mathbf{v_r}\} &= \mathrm{e}^{\mu}\{\mathbf{v_l}\} = \mathrm{e}^{\mathrm{j}kL_e}\{\mathbf{v_l}\}, \\ \{\mathbf{F_r}\} &= -\mathrm{e}^{\mu}\{\mathbf{F_l}\} = -\mathrm{e}^{\mathrm{j}kL_e}\{\mathbf{F_l}\}. \end{aligned} \tag{2}$$

δ is the attenuation constant and ε is the phase constant [17, p. 187]. The complex wavenumber k with the real part defining the phase difference per unit length and the imaginary part the attenuation per unit length, is included in Eq. (2) in conjunction with the periodic length L_e.

Using the exponential ansatz of Eq. (2) in Eq. (1) and performing some algebraic transformations results in a homogeneous matrix equation which has non-trivial solutions when the determinant of the matrix vanishes,

$$|\mathbf{Y_{ll}} + \mathbf{Y_{rr}} - \mathrm{e}^{\mu}\mathbf{Y_{lr}} - \mathrm{e}^{-\mu}\mathbf{Y_{rl}}| = 0. \tag{3}$$

At any frequency, up to $2n_{\mathrm{dof}}$ different values of μ can exist. To each eigenvalue corresponds certain eigenvectors for $\mathbf{F_l}$ and $\mathbf{v_l}$.

The phase constant related to propagating waves is multi-valued. If ε_0 is a solution between 0 and π, then $\varepsilon_n = \varepsilon_0 + 2\pi n$ $(n = 0, \pm 1, \pm 2, \pm 3 \ldots)$ is also a solution to Eq. (3).

The phase constant has a distinct relation to the wavenumber as it represents the difference in phase of the motion in the periodic system at points separated by the periodic distance L_e. The corresponding phase difference per unit length (wavenumber k_n) is ε_n/L_e,

$$k_n = \pm(2n\pi + \varepsilon_0)/L_e. \tag{4}$$

As a result of the multi-valued travelling components, an infinite series of (harmonic) waves with the given wavenumbers exists in the periodic system. The positive and negative wavenumbers are related to left- and rightwards travelling waves, respectively.

In analogy to the wavenumber definition for travelling waves, an imaginary wavenumber component for the decaying waves can be defined by

$$k_{\mathrm{decay}} = \pm\mathrm{j}\delta/L_e. \tag{5}$$

In contrast to the multi-valued solution for the travelling waves, the decaying waves are single valued.

From the solution of the determinantal equation (3) the wavenumbers can be directly calculated. For each characteristic wave the distribution is fixed between the principal value and the higher and lower values of ε_n or k_n. However, the overall wavenumber content for a certain excitation depends not only on the structure itself but also on the amplitudes of the excited characteristic waves. Each characteristic wave contributes to the overall wavenumber spectrum through its definite wavenumber content, weighted with its wave amplitude. This definite wavenumber content is detailed in Section 4.

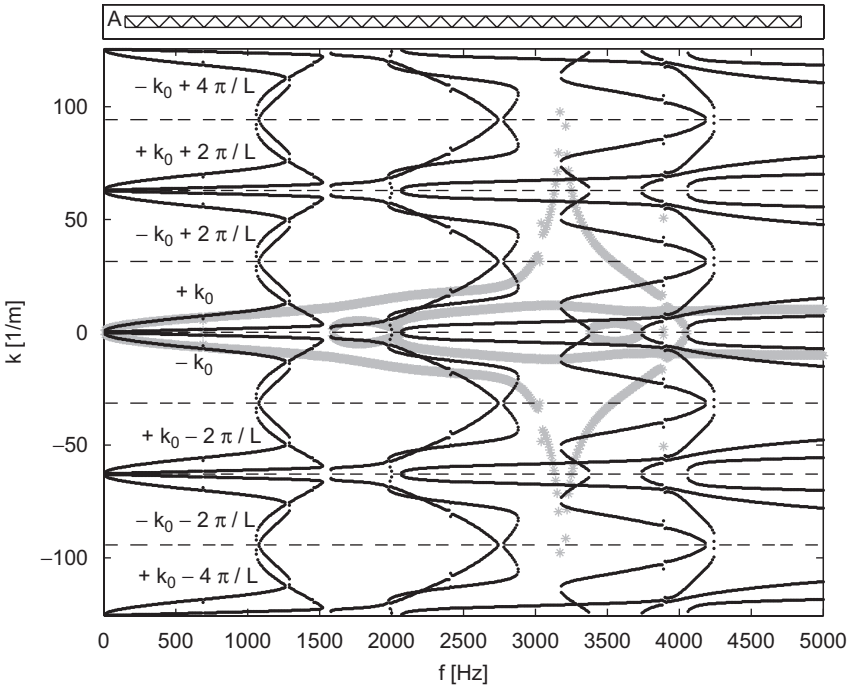

Fig. 3. Wave number dispersion plot for periodic profile strip A including positive, negative travelling waves and decaying waves (* (grey): decaying waves, ... (black): propagating waves).

Herein, the solution of the determinantal equation (3) is limited to purely real or imaginary wavenumbers. Hence, only the purely propagating and decaying waves are shown in Fig. 3 for strip A. Complex waves are not included.

As the wavenumber is periodically repeated with $2n\pi/L_e$, only a fraction of the complete dispersion diagram can be shown and indeed, there is no benefit of plotting more than $\pm k_0$ except for the decaying part, plotted in gray, which is not periodic (imaginary wavenumber).

In order to illustrate the periodic character of the propagating waves the plot is extended beyond the principal values. Regions in the plot indicate (repeated) rightward or leftward travelling waves.

A drawback of the approach with the determinantal equation relates to the complex valued solutions. Thereby the wave comprises a propagating and a decaying part. It is a quite laborious task to find the complex roots of the determinantal equation for each frequency. Hence, for the complete picture including complex waves, the approach using the transfer matrix presented later is favourable.

2.2. Dispersion characteristics using spatial Fourier transform

For this approach a spatial sampling at discrete points is necessary, resulting in the discrete Fourier transform (DFT). Having a profile of length L with N equally distributed spatial sampling points, $v_q = v(q\Delta x);\ q = 1, 2, 3, \ldots, Q$, results in the following transformation:

$$\begin{aligned} V_p = V(p\Delta k) &= \Delta x \sum_{q=1}^{Q} v_q \mathrm{e}^{-\mathrm{j}2\pi(pq/Q)}, \quad p = 1, 2, 3, \ldots, Q \\ &= \Delta x \sum_{q=1}^{Q} v_q \mathrm{e}^{-\mathrm{j}2\pi p \Delta k x_q}, \quad \Delta k = \frac{2\pi}{L} = \frac{2\pi}{Q\Delta x}. \end{aligned} \tag{6}$$

To satisfy the Nyquist criterion, the maximum wavelength, which can be unambiguously identified, is given by $k_{\max} = 1/2\Delta x$. Therefore, it has to be assured that there is only negligible spectral content above this

wavenumber. This can only be done by choosing a high resolution so that the critical wavenumber is above the highest occuring wavenumber.

The advantage of the DFT-approach is that it is easy to implement. Standard FFT algorithms can be used and it is applicable to all profile structures independent of periodicity. The disadvantage is that it is computational quite demanding as the complete vibration field of the profile has to be calculated and the FFT with high resolution has to be performed. One problem for finite structures is that the wavenumber resolution depends only on the investigated profile length L. For an adequate resolution a long profile strip has to be calculated enlarging the computational effort involved.

Another feature of this approach is that the energy distribution in the periodic wavenumber series is readily obtained. This gives some remarkable insight for the given excitation conditions as the excitation of different wave types can be identified. On the other hand, it should be pointed out that this can also give misleading results when trying to extract the general wave propagation features. Not all possible wave types in the structure need to be excited by a certain force or moment excitation. At least, different excitation mechanisms should be applied and the results compared to get a more general picture.

The dispersion characteristics of the profile strip A using the DFT approach are shown in Figs. 4 and 5 for force and moment excitation, respectively. The excitation is located at the left end of the profile strip, the right end is damped with gradually increasing loss factor in order to simulate a non-reflective boundary comparable to a semi-infinite strip. The DFT is performed over a 6 m long section from the left end in order to achieve a good resolution.

For the DFT, the normal velocity distribution of the lower plate is calculated and interpolated to give a uniform spatial sampling by using a spline interpolation function.

The result of the spatial Fourier transform is given by the two-sided spectrum V of the velocity distribution. For plotting the logarithmic value of the magnitude $L_{v,\mathrm{DFT}} = 20\log[|V|/(5\mathrm{e}-8\,\mathrm{m/s})]$ is used.

Despite the simulated non-reflective boundary on the right, reflections occur in the low-frequency regime and hence, modes are visible, manifested by faint vertical lines up to about 1000 Hz.

The periodic nature of the wavenumber content is visible when using the DFT, but the energy is distributed in a characteristic way between the principal value and the 'side bands'. The DFT-results for profiles B and C are not shown for the sake of brevity.

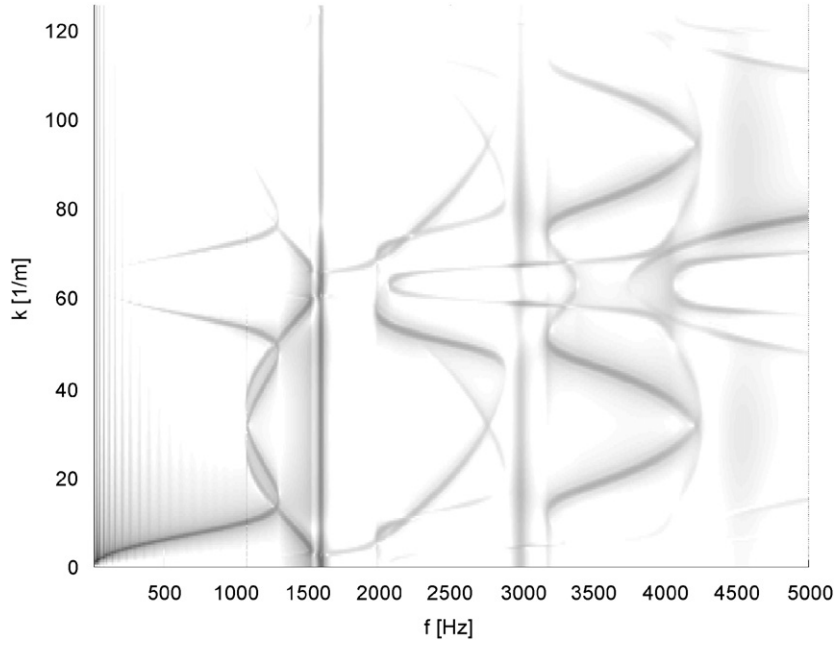

Fig. 4. DFT plot of lower plate profile A, unit force excitation at left lower side, shading limits $L_{v,\mathrm{DFT}}$: 10 (white) ... 90 (black) dB re. $5\mathrm{e}-8\,\mathrm{m/s}$.

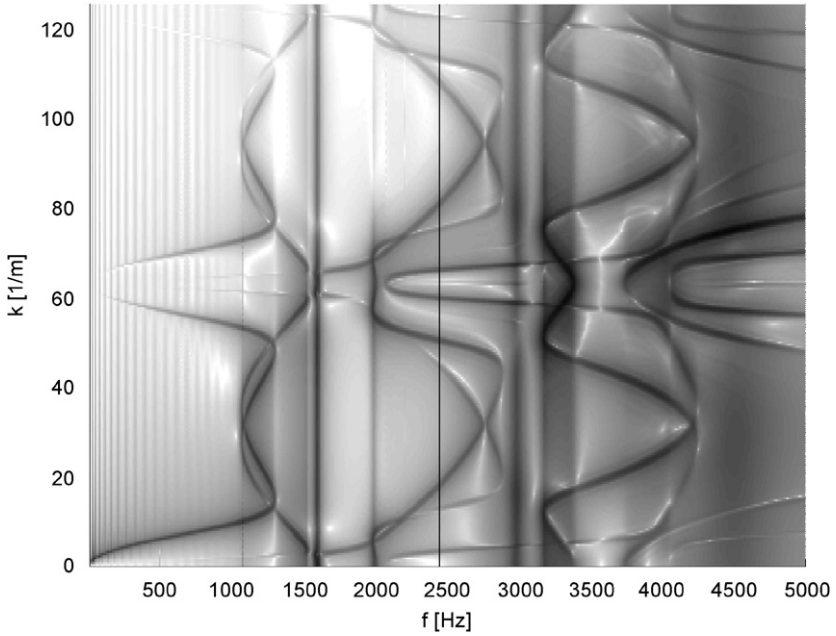

Fig. 5. DFT plot of lower plate profile A, unit moment excitation at left lower side, shading limits $L_{v,\mathrm{DFT}}$:10 (white) ... 90 (black) dB re. 5e − 8 m/s.

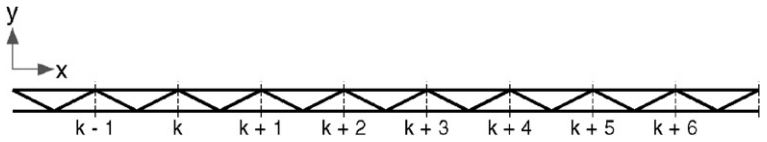

Fig. 6. The positions along the periodic chain are labelled in the given way.

The decaying waves cannot be found in the DFT-result as they decay too rapidly and do not contribute significantly to the velocity spectrum of the complete strip. They can be extracted using the determinantal equation or by solving the eigenvalue problem. This gives a clearer picture of the characteristic waves, but the energy distribution cannot be extracted directly.

2.3. Dispersion characteristics using transfer matrix eigenvalue problem

As an alternative for finding the wave types in the periodic structure, the transfer matrix $\mathbf{T}$ of a single subsystem can be used. The notation for the positions along the periodic chain is shown in Fig. 6.

Starting with the definition of the T-matrix

$$\begin{Bmatrix} \mathbf{v_{k+1}} \\ \mathbf{F_{k+1}} \end{Bmatrix} = \mathbf{T} \begin{Bmatrix} \mathbf{v_k} \\ \mathbf{F_k} \end{Bmatrix} \tag{7}$$

and invoking Bloch's theorem, Eq. (2), the state vectors on both sides of the periodic subsystem can be related by

$$\begin{Bmatrix} \mathbf{v_{k+1}} \\ \mathbf{F_{k+1}} \end{Bmatrix} = \lambda \begin{Bmatrix} \mathbf{v_k} \\ \mathbf{F_k} \end{Bmatrix}, \quad \text{where } \lambda = \mathrm{e}^{\mu}. \tag{8}$$

Combining Eqs. (7) and (8) results in an eigenvalue problem, where the identity matrix $\mathbf{I}$ is introduced,

$$[\mathbf{T} - \lambda \mathbf{I}] \begin{Bmatrix} \mathbf{v_k} \\ \mathbf{F_k} \end{Bmatrix} = \mathbf{0}. \tag{9}$$

From this equation it is obvious that λ are the eigenvalues of the T-matrix. The number of eigenvalues is two times the number of coupling coordinates. Routines for the solution of the complex eigenvalue problem are available and can be used to find all the eigenvalues and related propagation constants of the periodic system including the complex waves.

The only disadvantage of the approach apart from the multi-valued solution is the fact that numerical instabilities can arise in the solution of the eigenvalue problem. The multi-valued solution exists not only for the purely propagating waves, but also for the complex waves as $e^{\mu_{\text{complex}}} = e^{\mu_{\text{complex}}+2n\pi j}$, n being an arbitrary integer.

Due to the nature of the T-matrix, the eigenvalues are generally complex and occur in reciprocal pairs $(\lambda_i, 1/\lambda_i)$. Assuming no material dissipation, a purely propagating wave exists if $|\lambda_i| = 1$, corresponding to pass bands for the wave. In a stop band, the eigenvalues are real valued. An eigenvalue inside the unit circle represents a positive (right) going wave, whereas an eigenvalue outside the unit circle represents a negative (left) going wave.[1] Complex eigenvalues can occur only in groups of four and hence are only possible for systems with more than one coupling coordinate as there are only two eigenvalues for mono-coupled transfer matrices (2×2).

To each eigenvalue a certain eigenvector exists, defining the wave form of the wave type. The complete vibration of the profile can be set up by adding the contributions of all wave types

$$\begin{Bmatrix} \mathbf{v_k} \\ \mathbf{F_k} \end{Bmatrix} = \mathbf{\Phi_R^T} \begin{Bmatrix} \mathbf{L_k} \\ \mathbf{R_k} \end{Bmatrix}^{\mathrm{T}}. \tag{10}$$

As there are $2n_{\text{dof}}$ independent waves, the first n_{dof} columns of the matrix $\mathbf{\Phi_R}$ are the eigenvectors of the transfer matrix corresponding to the leftward travelling waves (λ_i, $i = 1, \ldots n_{\text{dof}}$, $\lambda_i \geqslant 1$) and the last n_{dof} columns the right-going waves ($1/\lambda_i$, $i = 1, \ldots n_{\text{dof}}$, $\lambda_i \geqslant 1$). n_{dof} defines the number of coupling coordinates with corresponding orthogonal eigenvectors, excluding the pass band bounding frequencies, where double eigenvalues occur.

The vector $\mathbf{L_k}$ contains the amplitudes of the left-going waves and the vector $\mathbf{R_k}$ contains those of the right-going waves. The wave amplitudes at adjacent bays are related by

$$\begin{Bmatrix} \mathbf{L_{k+1}} \\ \mathbf{R_{k+1}} \end{Bmatrix} = \mathbf{W} \begin{Bmatrix} \mathbf{L_k} \\ \mathbf{R_k} \end{Bmatrix} \quad \text{where } \mathbf{W} = \mathbf{\Phi_R^{-1}} \mathbf{T} \mathbf{\Phi_R}. \tag{11}$$

Since $\mathbf{\Phi_R}$ is the (right) eigenvector matrix of $\mathbf{T}$, the matrix $\mathbf{W}$ is the diagonal matrix of the eigenvalues of $\mathbf{T}$ and is called the wave transfer matrix,

$$\mathbf{W} = \begin{bmatrix} \mathbf{\Lambda} & \mathbf{0} \\ \mathbf{0} & \mathbf{\Lambda^{-1}} \end{bmatrix} \quad \text{where } \mathbf{\Lambda} = \text{diag}(\lambda_1, \ldots, \lambda_m). \tag{12}$$

Solving the eigenvalue problem in Eq. (9) results in a complete picture of free wave propagation in the strip. The eigenvalues can be directly linked to wavenumbers and the eigenvectors establish the wave form of each characteristic wave. Knowing the wave amplitudes at a certain position makes it possible to calculate the complete wave amplitudes at all other positions along an infinite strip using the wave transfer matrix

[1] This distinction is not possible for undamped systems, where in the passbands $|\lambda| = 1$. In this case the distinction can be based on the following rule provided $e^{j\omega t}$:

$$\text{Im}(\lambda) > 0 \rightarrow k \text{ positive} \rightarrow \text{negative (left) travelling wave},$$

$$\text{Im}(\lambda) = 0 \rightarrow k = 0 \rightarrow \text{standing wave},$$

$$\text{Im}(\lambda) < 0 \rightarrow k \text{ negative} \rightarrow \text{positive (right) travelling wave}.$$

containing the eigenvalues. In practice it is necessary to get the wave amplitudes for a certain excitation (forced response). This is treated in Section 5.

The major task after the solution of the transfer matrix eigenvalues is the identification of the different characteristic wave types, i.e. the unique separation of the wave types over the whole investigated frequency range. Different algorithms are tried in the complex plane for the propagation constants, but fail mainly at the points where different wave types join. A unique separation at these points is difficult (or perhaps not possible) if the structural dissipation is set to zero. By adding a small amount of structural dissipation ($\eta = 0.01$) it is possible to follow each characteristic wave in the complex plane, as the coupling of the wave types is reduced. This is in accordance with the findings for reduced flexural-longitudinal wave coupling in Ref. [18]. The eigenvalues are identified as complex conjugate pairs and only the eigenvalues with modulus smaller than unity are taken for the identification procedure. The sorted frequency dependent wavenumber content for the right-travelling waves 7–12 is shown for strips A–C in Figs. 7–9.

It is obvious that the profiles with inclined members (A and B) exhibit a more involved wave propagation. Low-frequency bending wave dispersion for the equivalent beam defined in Ref. [16] can be identified for waves 11 (A) and 10 (B) up to about 1000 Hz. For strip A, longitudinal wavenumbers can be identified in wave 8 in the range 2000–4000 Hz. Wave 10 exhibits longitudinal character for strip B between 1000 and 2500 Hz. Hence, it is clear that the character of a wave can change with frequency. For strip C this kind of change does not occur; waves 11 and 12 stay longitudinal in the frequency range up to 4000 Hz. Wave 7 of strips A and B is a purely decaying wave having a wavenumber outside the plotted range. This marked decaying process (or growing process when regarded in the other direction) leads to numerical instability, clearly visible in the high-frequency regime. For Profile C waves 7–10 exhibit a strong decaying component in wide frequency ranges. Wave 10 propagates only in some frequency bands, whereas wave 9 only around 1500 Hz. Above 4000 Hz both are propagating. Only the mainly longitudinal waves 11 and 12 are propagating in almost the complete frequency range.

3. Characteristic waves

In order to plot the wave forms, the eigenvectors, including the end point velocities and forces, are used to calculate the complete velocity pattern of the intermediate beams. For subelements without internal joints, this can be done straightforwardly. For others, the transfer matrix of a part of the element has to be adopted to calculate the intermediate state vectors from which the complete pattern can be reconstructed.

The resulting characteristic waves are shown in Figs. 10–12 for a frequency of 1000 Hz. For profile A the waves 11 and 12 are propagating whilst the other wave types are either purely decaying or complex. For practical applications, the propagating waves will dominate the overall vibration of the plate strips. Wave 11, which can be characterized mainly by a form of bending vibration, shows a clear mixture of global and local displacements. Wave 12 is a propagating compressional wave that also contains long and short wavelength components.

For profile B wave types 8 and 12 are mainly propagating. Wave 8 is of compressional character and wave 12 is a mixture of long wave bending and compressional wave.

The propagating waves of profile C at 1000 Hz are number 11 (rotational wave) and 12 (compressional wave).

It should be kept in mind, that no strict classification of the wave types over the complete frequency range can be achieved as e.g. wave number 8 of profile A starts as a decaying wave at low frequencies, then reaches a propagation zone with bending character, is complex again, turns into a compressional wave that passes over in a bending type wave, and finally gets complex again in the investigated frequency range up to 5000 Hz (see Fig. 7).

The identification of the characteristic waves realizes the opportunity to simplify the wave propagation in the profile strips. It is reasonable, that the decaying and complex waves do not contribute significantly to the overall vibration of the panel, at least if there is a limited number of excitation points such that the waves can decay.

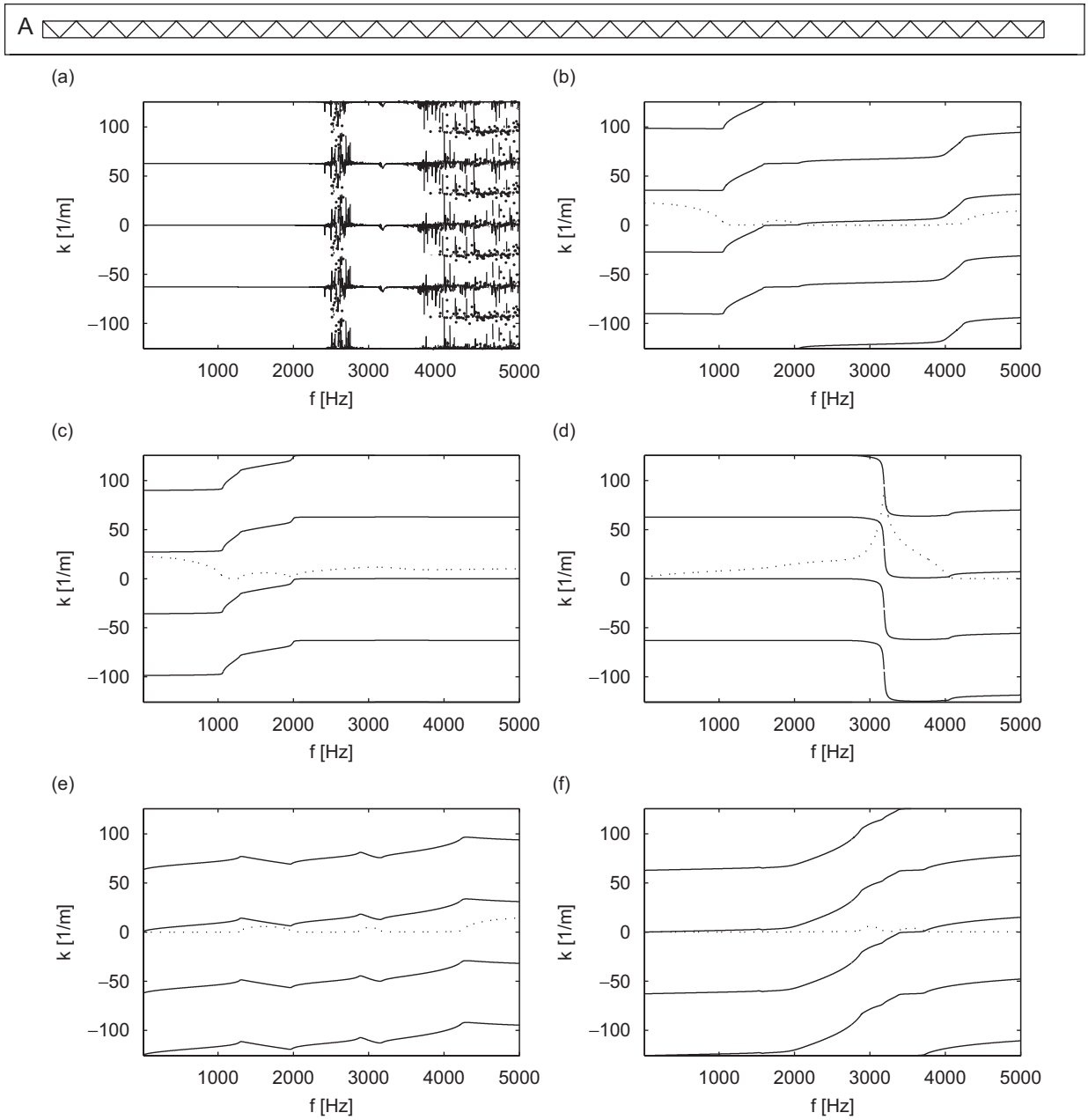

Fig. 7. Wavenumbers of characteristic waves of profile A extracted using T-matrix, (a) Wave 7, (b) Wave 8, (c) Wave 9, (d) Wave 10, (e) Wave 11, (f) Wave 12, — propagating, - - decaying.

4. Wavenumber content in characteristic waves

4.1. Theory

When looking at the wave forms of the profile strips it is obvious that the non-uniqueness of the wavenumbers, resulting from the solution of the eigenvalue problem, is only part of the truth. It establishes a set of *possible* wavenumbers that mathematically fulfil the periodic system condition. The distribution among these wave set components is fixed and can be extracted for each characteristic wave.

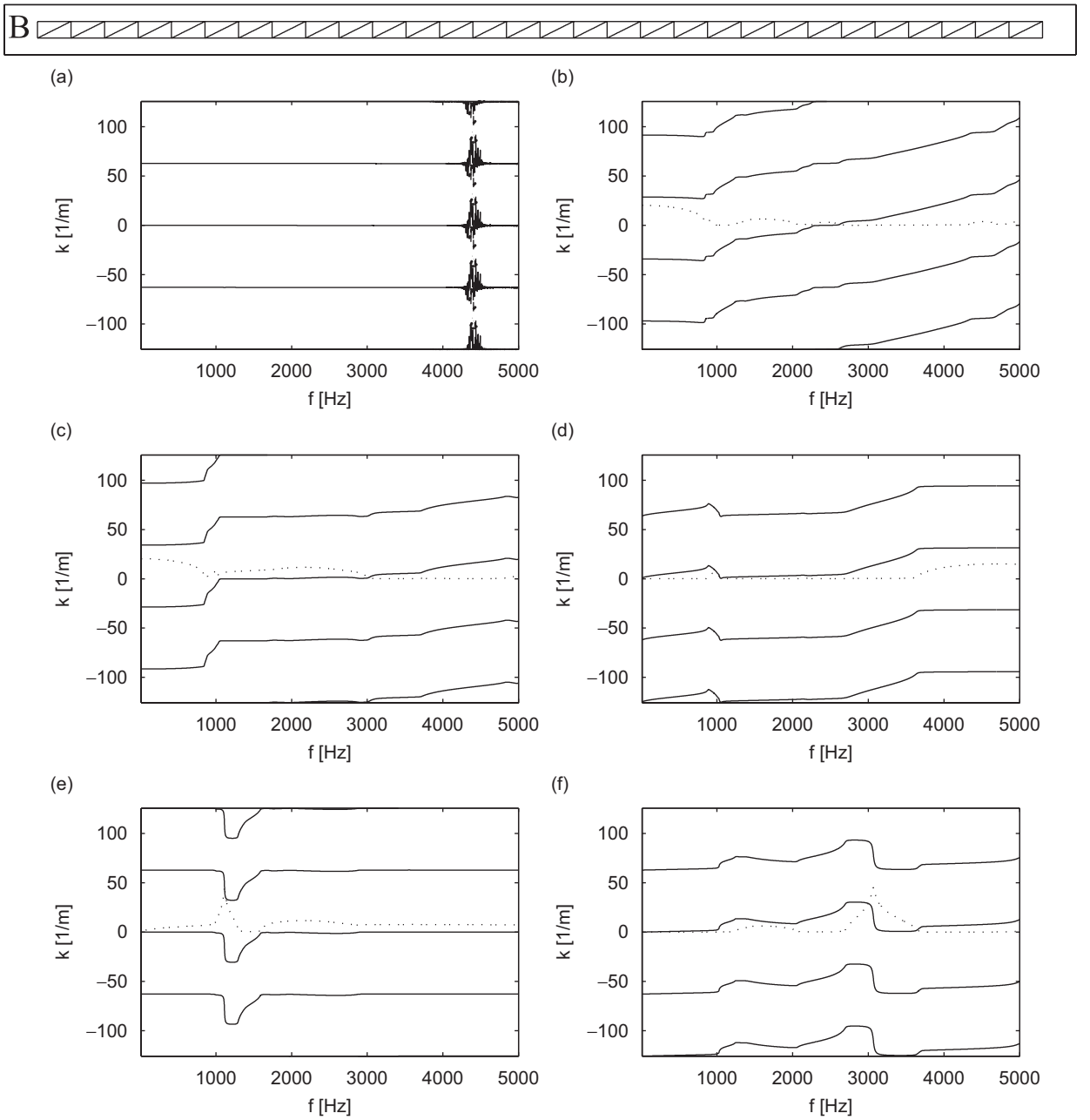

Fig. 8. Wavenumbers of characteristic waves of profile B extracted using T-matrix, (a) Wave 7, (b) Wave 8, (c) Wave 9, (d) Wave 10, (e) Wave 11, (f) Wave 12, — propagating, - - decaying.

The mathematical non-uniqueness for the wavenumbers (periodicity of $2\pi/L_e$) can be explained by the limited spatial resolution of the real physical process. It is not possible to distinguish—with a spatial sampling of L_e—if in between two neighbouring endpoints of the subsystem, e.g. one or two wavelengths occur. For a general phase shift ε from point to point this means that adding 2π does not change the results at the sampling points $e^{j\varepsilon} = e^{j(\varepsilon+n2\pi)}$. In terms of wavenumbers $k_n = k_0 + n2\pi/L_e$.

In contrast to this mathematical ambiguity the physical wavenumber distribution on the structure has to be definite, which means that the energy distribution among the corresponding possible wavenumbers is fixed. It is reasonable that for each characteristic wave such a wavenumber distribution can be determined regardless

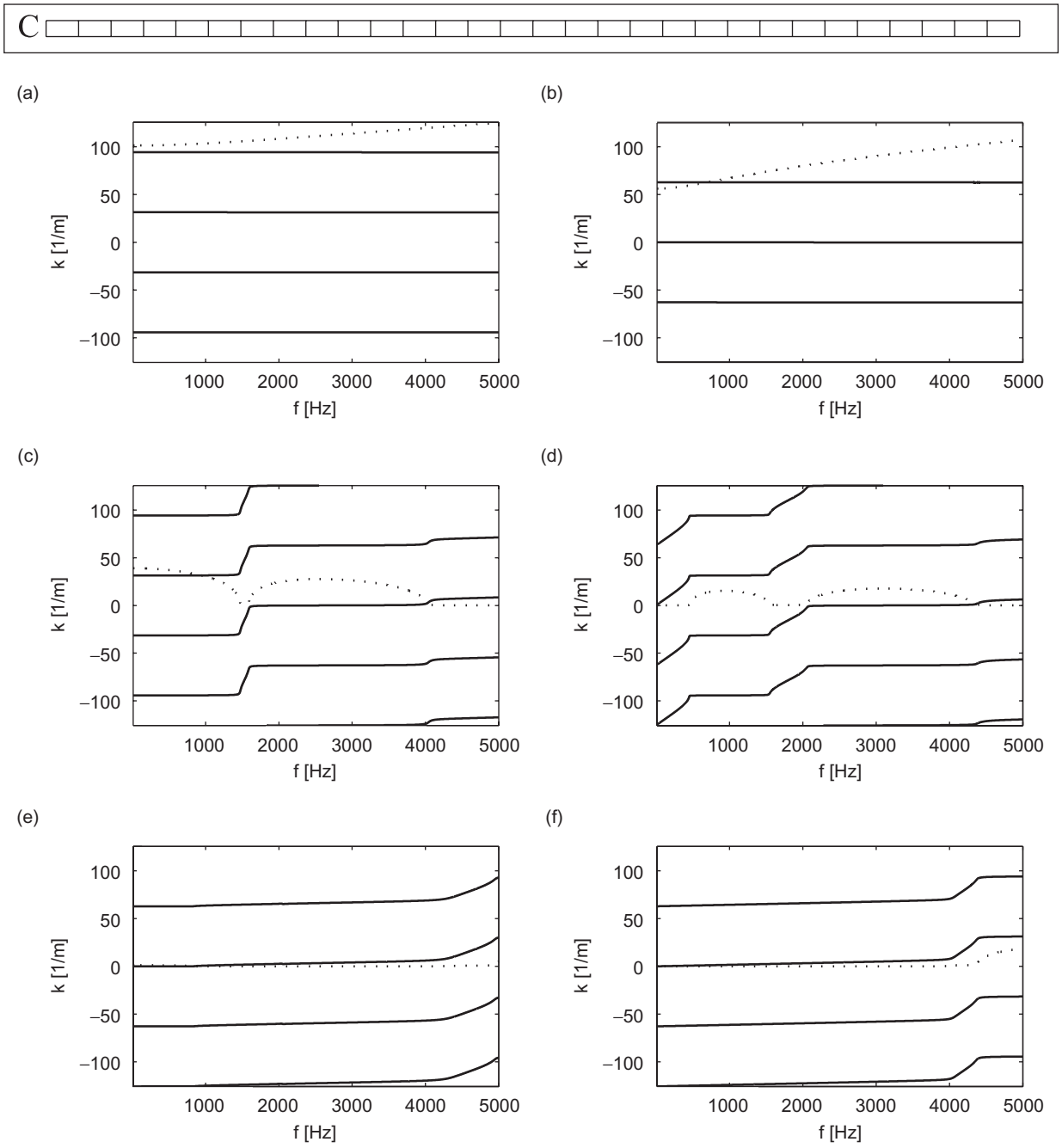

Fig. 9. Wavenumbers of characteristic waves of profile C extracted using T-matrix, (a) Wave 7, (b) Wave 8, (c) Wave 9, (d) Wave 10, (e) Wave 11, (f) Wave 12, — propagating, - - decaying.

of the excitation mechanism. The excitation only determines the characteristic wave amplitudes and not the distribution of wavenumbers in each characteristic wave. Hence, it is possible to calculate the fixed wavenumber distribution in each characteristic wave from a characteristic wave form.[2] Summing up the

[2]The distribution depends not only on the characteristic wave itself but also on the component of motion of interest. For sound radiation to the exterior the normal velocity of the outer plates is sought. The wavenumber distribution for vibrations in the x-direction will probably be significantly different!

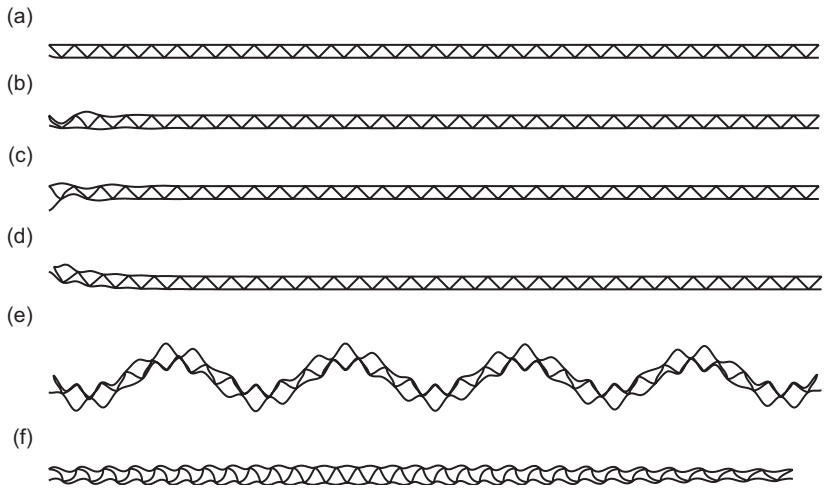

Fig. 10. Wave forms of characteristic right-travelling waves for profile A ($f = 1000\,\mathrm{Hz}$), (a) Wave 7, (b) Wave 8, (c) Wave 9, (d) Wave 10, (e) Wave 11, (f) Wave 12.

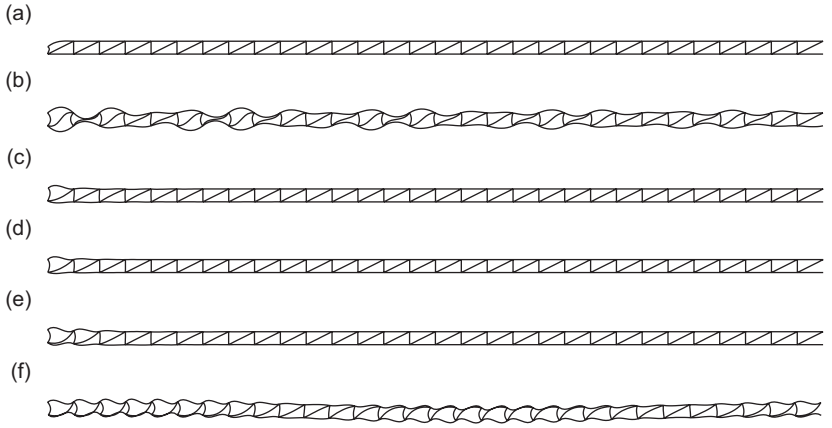

Fig. 11. Wave forms of characteristic right-travelling waves for profile B ($f = 1000\,\mathrm{Hz}$), (a) Wave 7, (b) Wave 8, (c) Wave 9, (d) Wave 10, (e) Wave 11, (f) Wave 12.

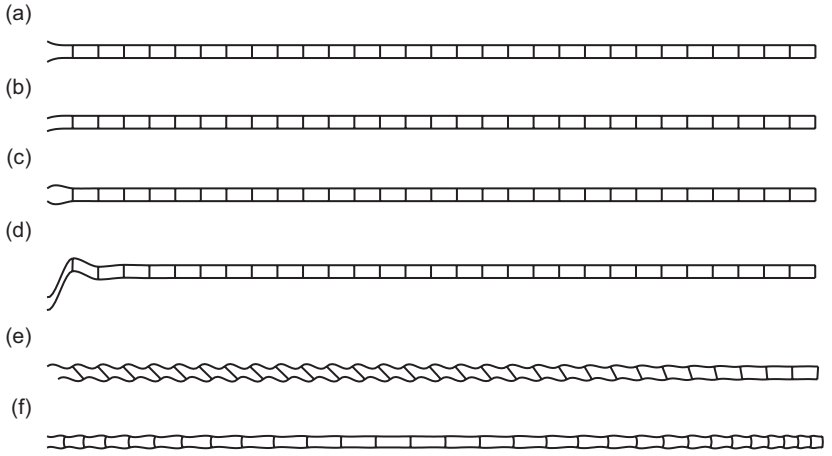

Fig. 12. Wave forms of characteristic right-travelling waves for profile C ($f = 1000\,\mathrm{Hz}$), (a) Wave 7, (b) Wave 8, (c) Wave 9, (d) Wave 10, (e) Wave 11, (f) Wave 12.

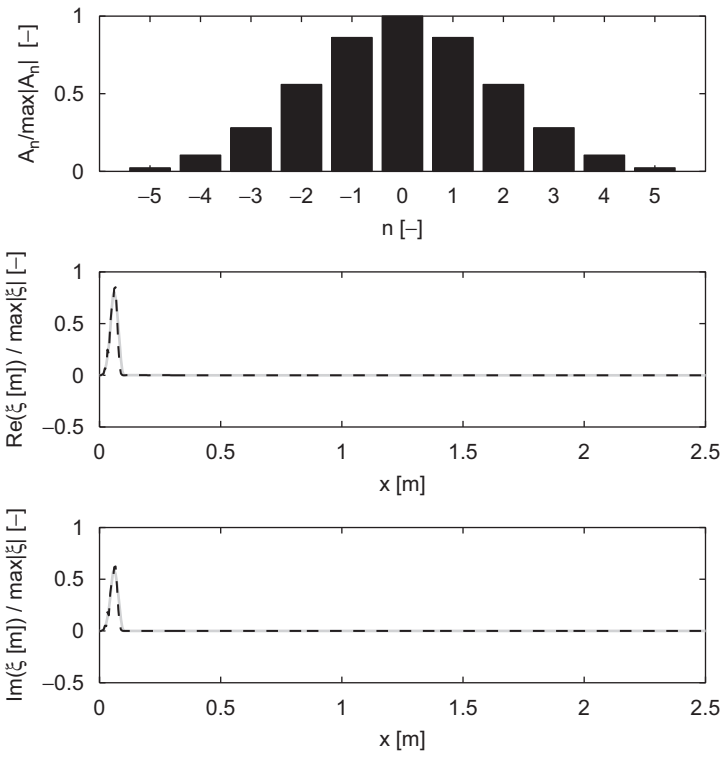

Fig. 13. Wave amplitudes of space harmonic series (Profile A, $f = 1000$ Hz, wave 7, — calculated displacement (grey) - - wave series fit (black).

contributions of all excited characteristic waves results in a unique wavenumber spectrum of the strip that can be used, e.g. for the calculation of sound radiation.

One option to extract the frequency-dependent wavenumber content, distributed in the set of wavenumbers is to perform a DFT of the characteristic wave forms. Though this approach is straightforward and easy to implement, there are the same general drawbacks as mentioned previously for the method. Additionally, for complex waves, the quantitative portions form a kind of mean value for the investigated range and hence the amplitudes depend strongly on the length of the transformed section. It is more desirable to get the wave amplitudes at a characteristic point ($x = 0$). With this information the displacement at any arbitrary position can be recalculated quite simple.

To circumvent the drawbacks mentioned for the DFT, it is possible for the periodic system to use another method. This is possible since some information about the wavenumbers and the inherent waves is available. The possible wavenumbers are known to be a series of wavenumbers, extracted from the transfer matrix eigenvalue problem. It is quite reasonable to assume that this series will converge rapidly since the main contributions will be in the range where the free wavenumbers occur in a simple homogeneous member. This is seen from the results presented later. Hence, another option is just to use the extracted wavenumber series as basis functions with unknown amplitudes. The amplitudes are estimated from the solution of $a(n)$ (overdetermined) linear system of equations by projecting the real displacement pattern to this wavenumber basis.

The displacement for a characteristic wave form to wave i at any point on the profile strip can be written as a series of 'space harmonics',

$$\boldsymbol{\xi}_{\mathbf{i}}(x) = \sum_{n=-\infty}^{\infty} A_{i,n}\boldsymbol{\varphi}_{\mathbf{i}}\mathrm{e}^{-\mathrm{j}k_{i,n}x} \quad \text{with } k_{i,n} = k_{i,0} + \frac{2n\pi}{L_e}. \tag{13}$$

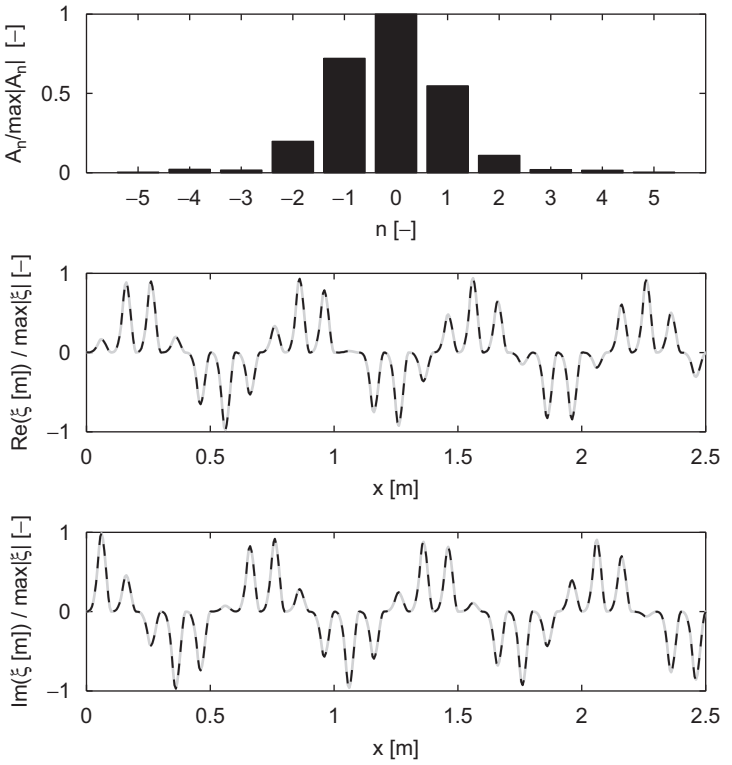

Fig. 14. Wave amplitudes of space harmonic series (Profile A, $f = 1000$ Hz, wave 11, — calculated displacement (grey) - - wave series fit (black).

In a reduced form considering only one direction, Eq. (13) holds also for the y-component, which is the relevant for the radiation,

$$\xi_{y,i}(x) = \sum_{n=-\infty}^{\infty} A_{i,n} \mathrm{e}^{-\mathrm{j}k_{i,n}x}. \tag{14}$$

The magnitude of the y-component in the eigenvector $\boldsymbol{\varphi}_\mathbf{i}$ is included in the wave amplitude $A_{i,n}$. This magnitude only affects the result with a constant factor, which is unimportant for the relative contributions of $k_{i,n}$. The correct scaling can be achieved by weighting the characteristic wave amplitudes in accordance with these relative contributions.

When truncating the series at M terms and using K positions for the displacement evaluation, Eq. (14) can be written for each characteristic wave in matrix form, omitting the wave index i,

$$\begin{Bmatrix} \xi_y(x_1) \\ \xi_y(x_2) \\ \cdots \\ \xi_y(x_K) \end{Bmatrix} = \begin{bmatrix} \mathrm{e}^{-\mathrm{j}k_{-M}x_1} & \mathrm{e}^{-\mathrm{j}k_{(-M+1)}x_1} & \cdots & \mathrm{e}^{-\mathrm{j}k_{M}x_1} \\ \mathrm{e}^{-\mathrm{j}k_{-M}x_2} & \mathrm{e}^{-\mathrm{j}k_{(-M+1)}x_2} & \cdots & \mathrm{e}^{-\mathrm{j}k_{M}x_2} \\ \cdots & & & \\ \cdots & & & \\ \mathrm{e}^{-\mathrm{j}k_{-M}x_K} & \mathrm{e}^{-\mathrm{j}k_{(-M+1)}x_K} & \cdots & \mathrm{e}^{-\mathrm{j}k_{M}x_K} \end{bmatrix} \cdot \begin{Bmatrix} A_{-M} \\ A_{-M+1} \\ \cdots \\ A_M \end{Bmatrix}.$$

$$(K,1) = \qquad (K, 2M+1) \qquad \times (2M+1, 1). \tag{15}$$

The number of displacement positions K must be greater or equal to $2M + 1$, i.e. the number of desired wave series amplitudes. If the number is greater, the system is overdetermined and can be solved using a least square solution routine. The spacing of the K displacement points is arbitrary but has to be chosen fine enough to ensure

a resolution necessary to represent the smallest occuring wavelength. It should be pointed out that the wave amplitudes as well as the displacements ξ are complex. Initially only the real part of ξ was used but then the method became unstable in some cases. This observation reveals that for a reliable reconstruction of the complex displacements of the characteristic waves the full information including both real and imaginary part is necessary.

4.2. Results

The relative amplitudes of profile A for selected characteristic waves travelling to the right (waves 7, 11 and 12) are shown in Figs. 13–15 for a frequency of 1000 Hz. For the results presented, the y-displacement of the upper outer beams is used and the amplitudes are normalized by the maximum amplitude. In order to check the implementation and the robustness of the method, a comparison is performed of real displacement shapes and reconstructed displacement shapes using the estimated wave series amplitudes.

It is clear that the method is robust in finding the relative wave series amplitudes; the matching between the calculated displacement and the wave series fit is that precise that the curves are hardly distinguishable in the plots. Moreover it can be stated, that in the investigated frequency range, $-5 \leqslant n \leqslant 5$ is sufficient to represent the wave forms. For the propagating waves, $-2 \leqslant n \leqslant 2$ could be sufficient as well. The amplitudes are not symmetric (equal for plus and minus n). This is due to the asymmetric nature of the subsystems.

A comparison is also done of the wave amplitude identification method and the DFT method. For the propagating waves, the spectra are quite similar as is seen in Fig. 16 but the discrepancy in amplitudes increases with wavenumber. For complex waves, the correct wavenumbers are found in the DFT, but the amplitude is underestimated because of the decaying process.

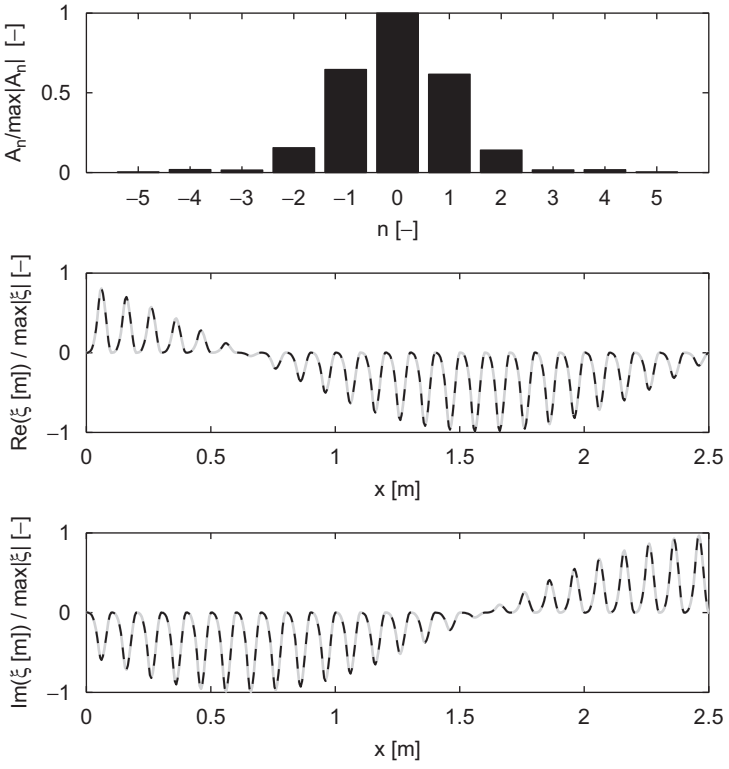

Fig. 15. Wave amplitudes of space harmonic series (Profile A, $f = 1000$ Hz, wave 12, — calculated displacement (grey) - - wave series fit (black).

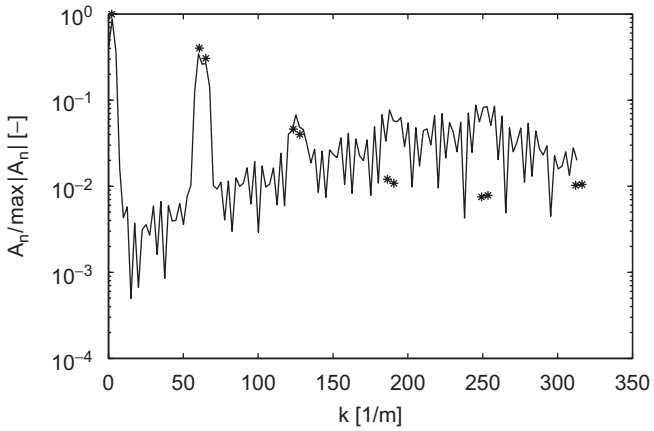

Fig. 16. Wave amplitudes of space harmonic series (*) in comparison to DFT result (—) (Profile B, $f = 1000$ Hz, wave 12).

The results up to now show only relative wave amplitudes for a frequency of 1000 Hz. In order to get an overview what happens in the complete frequency regime, shaded figures are created indicating the distribution of space harmonics for each wave. The plots are normalized by the maximum amplitude for each frequency and wave. These scaled results, in combination with the wave amplitudes for a forced response (see Section 5), lead to the quantitative space harmonic amplitudes for each wave and as a sum, the complete wavenumber distribution. The results for the waves propagating to the right (waves 7–12) are shown in Figs. 17–19. The plots illustrate the same real part of the wavenumbers as shown already in Figs. 7–9 for the characteristic waves. Additionally, the shading of the plots quantifies the relative contributions of each periodic wavenumber component. Dark zones indicate a dominance of this component whereas light shading indicates minor contribution to the wavenumber content of each characteristic wave.

It is obvious, that not only for 1000 Hz as shown previously, but also in the complete investigated frequency regime, the wavenumber content is localized between −200 and 200 1/m. Higher and lower wavenumbers contribute only minutely to the overall result. It is expected that the significant wavenumber group will gradually drift to larger values, if the behaviour were investigated for higher frequencies beyond 5000 Hz. For the presented positive travelling waves the group velocity is mainly positive (positive slope of the curves), also for the components with negative phase speed (negative wavenumber). This means that the space harmonic series gives a positive travelling characteristic wave (energy flow in positive direction) as a sum. However, there are some components with negative phase speed included, induced by the reflections at the joints. There are, indeed, some characteristic waves with negative group velocity in some frequency ranges, e.g. wave 11 of profile A between 1400 and 2000 Hz.

5. Forced response of infinite profile strip

For structural acoustic investigations in the mid and high Helmholtz number regime, theoretical infinite systems are of great value. In those regimes the influence of boundary effects for finite structures diminishes such that the corresponding infinite structure can be used to estimate the behaviour of the former. Hence, forced excitation of infinite strips is investigated here.

According to Engels [19] the forced response of an infinite or semi-infinite periodic structure can be calculated based on the eigenvalues and eigenvectors of the transfer matrix. An alternative is the direct use of the dynamic stiffness matrix of the subsystem, outlined by Thompson [20] to calculate the wavenumbers and forced response of a structure, applied and extended also in Ref. [21]. For the present study, the employed slope-deflection method directly establishes the dynamic stiffness matrix. Hence, this alternative is selected for the eigenvalue problem.

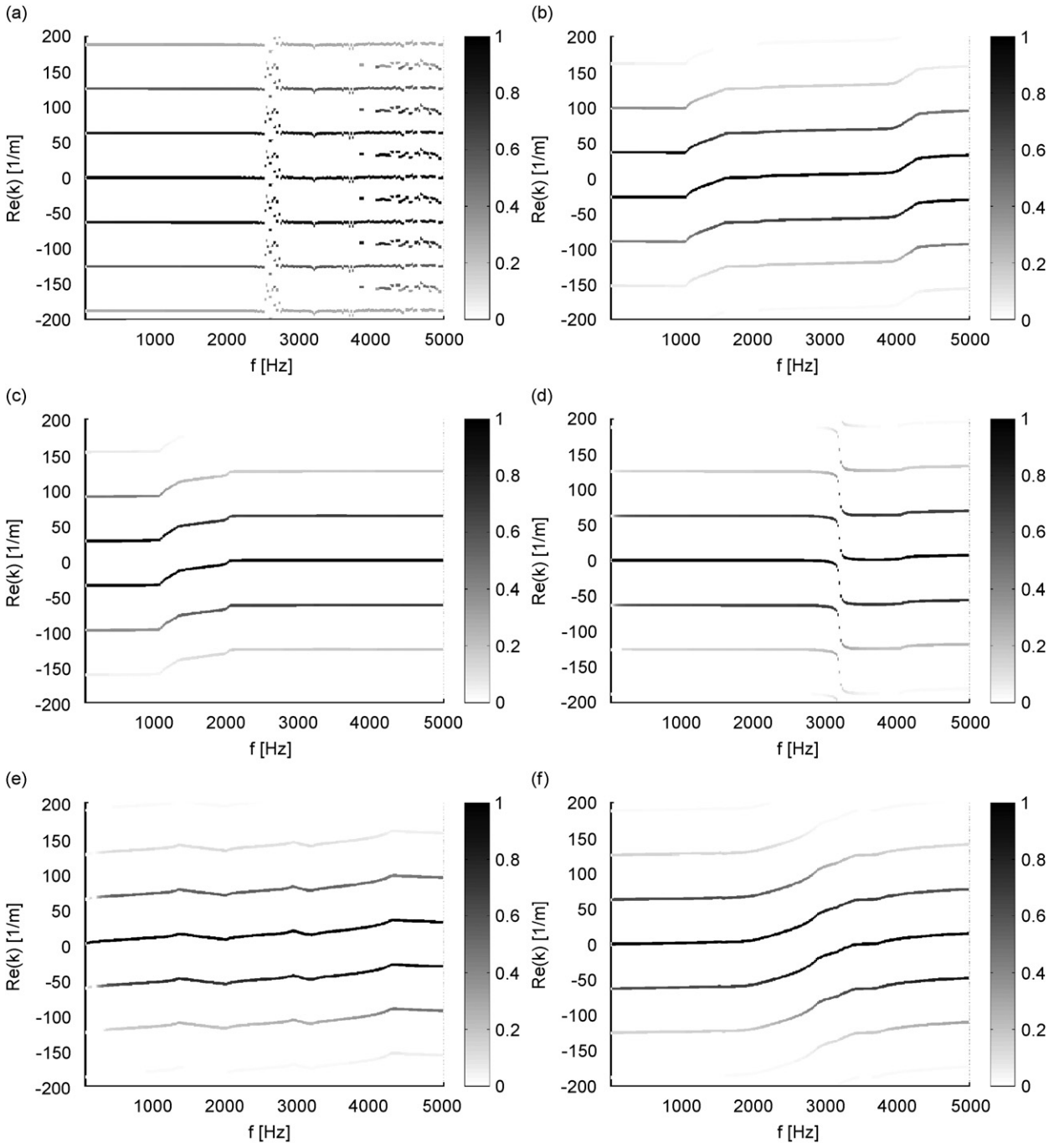

Fig. 17. Normalized wave amplitudes of space harmonic series (Profile A), (a) Wave 7, (b) Wave 8, (c) Wave 9, (d) Wave 10, (e) Wave 11, (f) Wave 12.

5.1. Theory of forced response using dynamic stiffness matrix

For the infinite periodic strip, forced response can be developed by using the dynamic stiffness matrix of a single subsystem [20]. If the periodic subsystem contains inner dofs which are not connected to the left or right side, it is necessary to build a new reduced dynamic stiffness

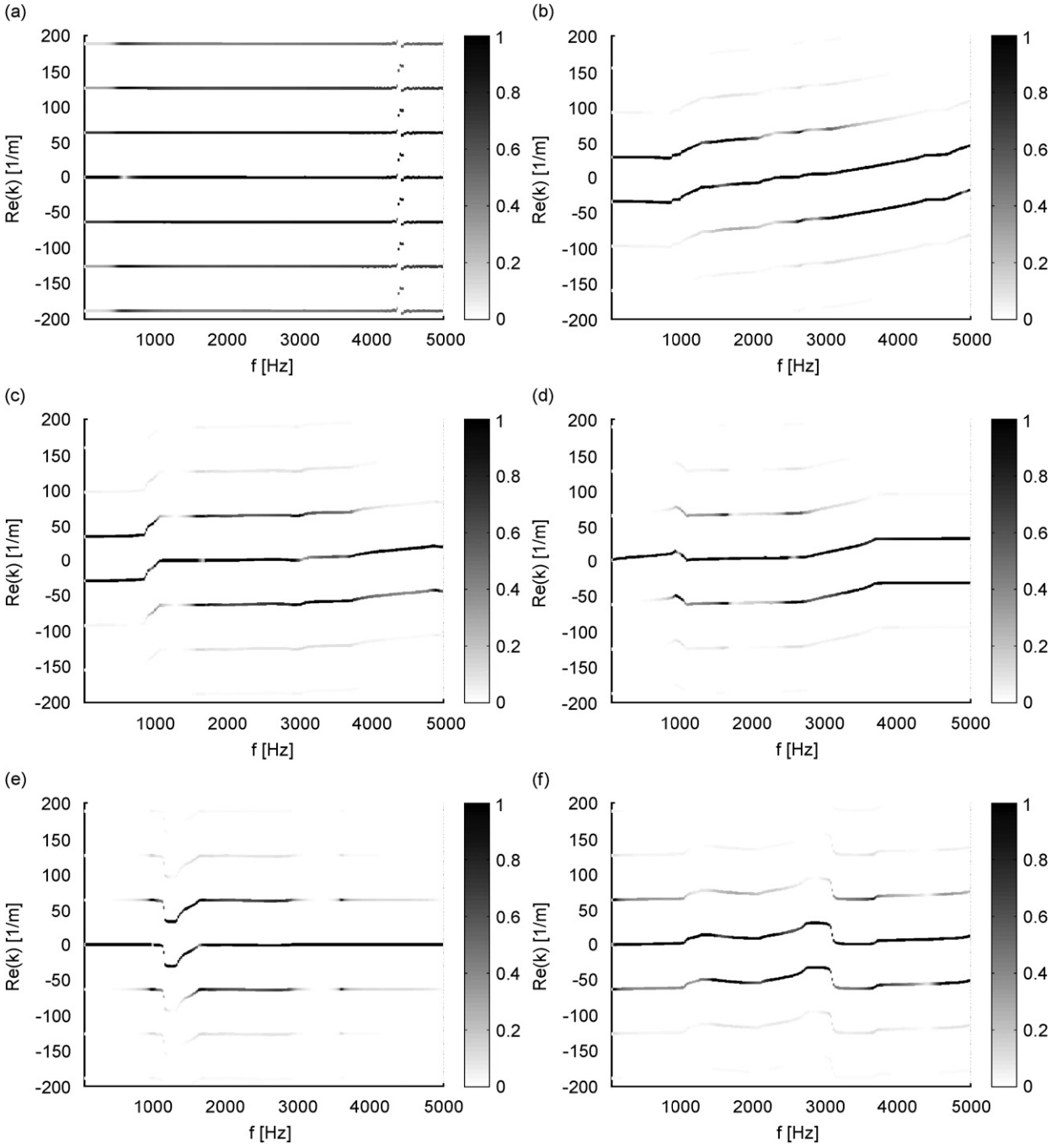

Fig. 18. Normalized wave amplitudes of space harmonic series (Profile B), (a) Wave 7, (b) Wave 8, (c) Wave 9, (d) Wave 10, (e) Wave 11, (f) Wave 12.

matrix as the matrix elements depend on the chosen dofs (blocked terminals). In contrast, the mobility enables arbitrary dofs to be eliminated without changing the remaining matrix elements. For the case with inner dofs, where no force excitation is assumed, the reduction starts with the definition of dynamic stiffness submatrices $\tilde{\mathbf{K}}$ where index i indicates inner dofs, l the left

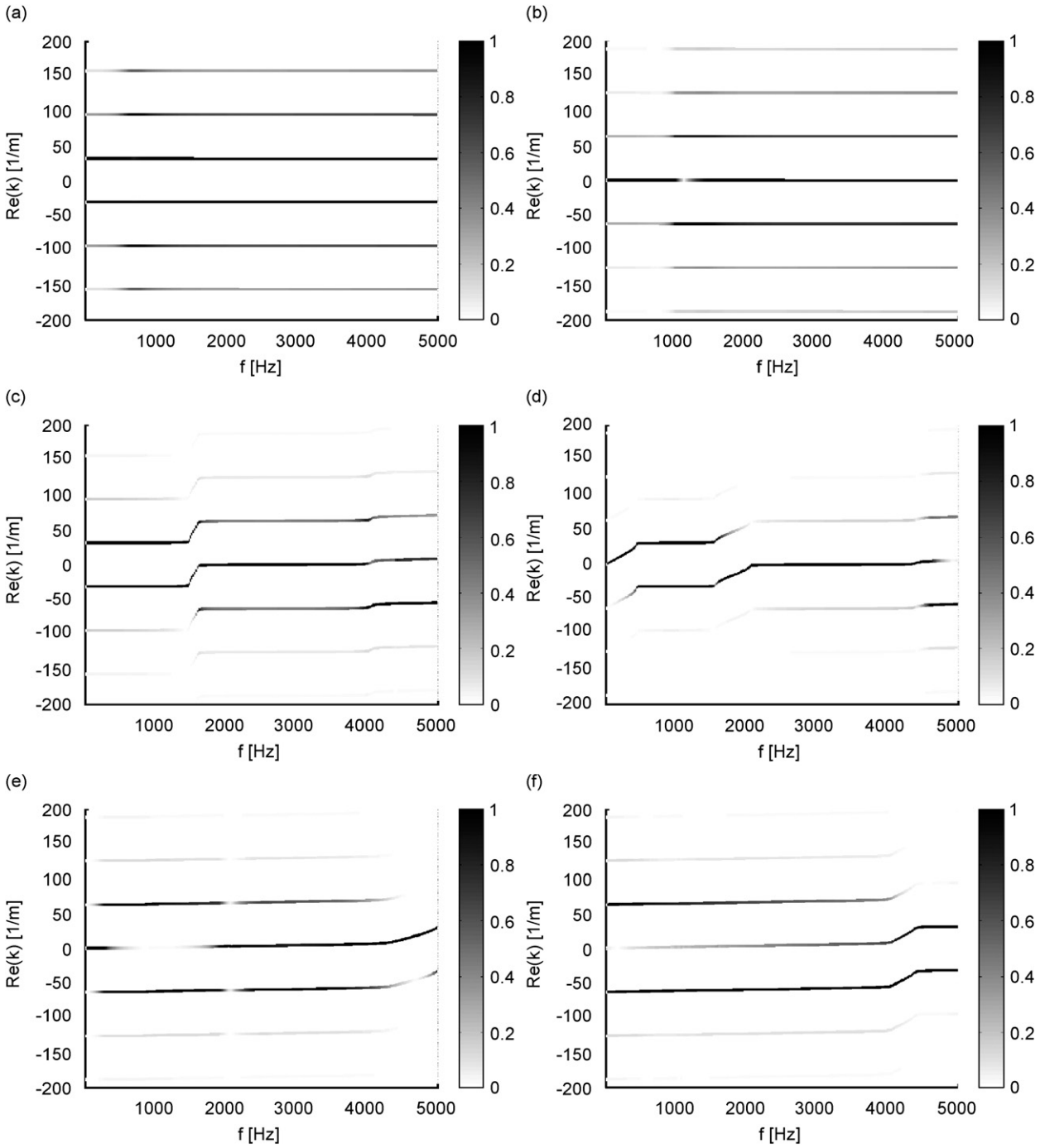

Fig. 19. Normalized wave amplitudes of space harmonic series (Profile C), (a) Wave 7, (b) Wave 8, (c) Wave 9, (d) Wave 10, (e) Wave 11, (f) Wave 12.

and r the right ones,

$$\begin{bmatrix} \tilde{\mathbf{K}}_{\mathbf{ll}} & \tilde{\mathbf{K}}_{\mathbf{li}} & \tilde{\mathbf{K}}_{\mathbf{lr}} \\ \tilde{\mathbf{K}}_{\mathbf{il}} & \tilde{\mathbf{K}}_{\mathbf{ii}} & \tilde{\mathbf{K}}_{\mathbf{ir}} \\ \tilde{\mathbf{K}}_{\mathbf{rl}} & \tilde{\mathbf{K}}_{\mathbf{ri}} & \tilde{\mathbf{K}}_{\mathbf{rr}} \end{bmatrix} \begin{Bmatrix} \boldsymbol{\xi}_{\mathbf{l}} \\ \boldsymbol{\xi}_{\mathbf{i}} \\ \boldsymbol{\xi}_{\mathbf{r}} \end{Bmatrix} = \begin{Bmatrix} \mathbf{F}_{\mathbf{l}} \\ \mathbf{0} \\ \mathbf{F}_{\mathbf{r}} \end{Bmatrix}. \tag{16}$$

The inner dofs can be eliminated by using the relation

$$\xi_i = -\tilde{\mathbf{K}}_{ii}^{-1}(\tilde{\mathbf{K}}_{il}\xi_l + \tilde{\mathbf{K}}_{ir}\xi_r). \tag{17}$$

After some simple algebraic manipulations the new dynamic stiffness matrix can be assembled as

$$\begin{bmatrix} \mathbf{K}_{ll} & \mathbf{K}_{lr} \\ \mathbf{K}_{rl} & \mathbf{K}_{rr} \end{bmatrix} \begin{Bmatrix} \xi_l \\ \xi_r \end{Bmatrix} = \begin{Bmatrix} \mathbf{F}_l \\ \mathbf{F}_r \end{Bmatrix}, \tag{18}$$

with

$$\begin{aligned} \mathbf{K}_{ll} &= \tilde{\mathbf{K}}_{ll} - \tilde{\mathbf{K}}_{li}\tilde{\mathbf{K}}_{ii}^{-1}\tilde{\mathbf{K}}_{il}, \quad \mathbf{K}_{lr} = \tilde{\mathbf{K}}_{lr} - \tilde{\mathbf{K}}_{li}\tilde{\mathbf{K}}_{ii}^{-1}\tilde{\mathbf{K}}_{ir} \\ \mathbf{K}_{rl} &= \tilde{\mathbf{K}}_{rl} - \tilde{\mathbf{K}}_{ri}\tilde{\mathbf{K}}_{ii}^{-1}\tilde{\mathbf{K}}_{il}, \quad \mathbf{K}_{rr} = \tilde{\mathbf{K}}_{rr} - \tilde{\mathbf{K}}_{ri}\tilde{\mathbf{K}}_{ii}^{-1}\tilde{\mathbf{K}}_{ir}. \end{aligned} \tag{19}$$

Based on Bloch's theorem Thompson gives the following eigenvalue problem $(\mathbf{B} + \lambda\mathbf{C})\mathbf{\Psi} = \mathbf{0}$ using the submatrices given in Eq. (19):

$$\left(\begin{bmatrix} \mathbf{K}_{rl} & \mathbf{K}_{rr} \\ \mathbf{0} & \mathbf{I} \end{bmatrix} + \lambda \begin{bmatrix} \mathbf{K}_{ll} & \mathbf{K}_{lr} \\ -\mathbf{I} & \mathbf{0} \end{bmatrix} \right) \begin{Bmatrix} \xi_l \\ \xi_r \end{Bmatrix} = \begin{Bmatrix} \mathbf{0} \\ \mathbf{0} \end{Bmatrix}. \tag{20}$$

After solving the eigenvalue problem for the eigenvalues λ and eigenvectors $\mathbf{\Psi}$, the solution can be arranged in a way such that the eigenvectors of right travelling waves are put into one submatrix $\mathbf{\Psi}^+$ containing the corresponding eigenvectors and another submatrix $\mathbf{\Psi}^-$ containing the left travelling components. Within each there are displacement dofs for the left part $\mathbf{\Psi}_l^{+/-}$ and the right part $\mathbf{\Psi}_r^{+/-}$ of the excited subsystem.[3]

The following equation relates the excitation forces at an arbitrary element within an infinite periodic structure to the wave amplitudes of the right travelling waves $\mathbf{R}$.[4]

$$\mathbf{F} = (\mathbf{K}_{ll}\mathbf{\Psi}_l^+ + \mathbf{K}_{lr}\mathbf{\Psi}_r^+ + \mathbf{K}_{rl}\mathbf{\Psi}_r^-\mathbf{\Psi}_l^{-^{-1}}\mathbf{\Psi}_l^+ + \mathbf{K}_{rr}\mathbf{\Psi}_l^+)\mathbf{R}. \tag{21}$$

This can be solved for the desired wave amplitudes $\mathbf{R}$ in the special excitation case by an inversion process once the excitation is specified.

The wave amplitudes of the left-travelling components can be deduced from the right-travelling amplitudes since [20]:

$$\mathbf{L} = \mathbf{\Psi}_l^-\mathbf{\Psi}_l^+\mathbf{R}. \tag{22}$$

These wave amplitudes in combination with the wavenumber content in each wave gives a quantitative description of the wavenumber content for a given excitation of an infinite profile strip.

5.2. Results for forced wave propagation of infinite strips

In this section, the theory outlined is used to extract the wave amplitudes of the characteristic waves for a given force (or moment) excitation of an infinite strip. The first step is the solution of the eigenvalue problem in this case based on the dynamic stiffness matrix of the corresponding subsystem. The eigenvectors, which are not velocity based in this case, but displacement based, are normalized with the vector (column) norm. After extracting the wave amplitudes for the left- and right-travelling normalized waves, the velocities at the excitation point can be calculated by using Eq. (10), resulting in the input mobility of the infinite strip. The same profiles used previously for the finite strips A–C are used as infinite profiles. Moreover, in order to benchmark the results, an approximate, infinite profile strip is investigated by directly assembling the complete dynamic stiffness matrix. This means that a weakly damped interior part (2.5 m, $\eta = 0.01$) is enclosed between two end parts where damping is slightly increased

[3]Note that the eigenvectors and the eigenvalue problem are defined here on a displacement basis. No forces are included in the eigenvectors.

[4]This seems to be the version given and used by Thompson. In the equation given by Brown the first two $\mathbf{\Psi}$ matrices in the third term are interchanged.

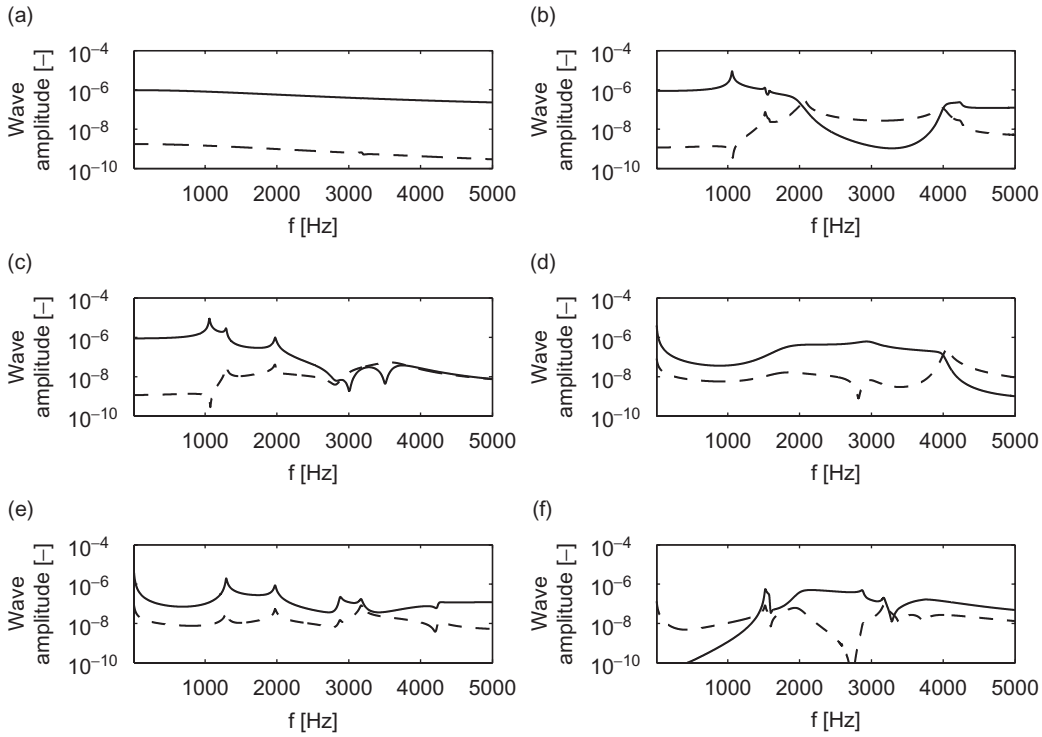

Fig. 20. Wave amplitudes of characteristic waves for force excited profile strip A, (– – $F_{1,x}$, — $F_{1,y}$), (a) Waves 1 & 7, (b) Waves 2 & 8, (c) Waves 3 & 9, (d) Waves 4 & 10, (e) Waves 5 & 11, (f) Waves 6 & 12.

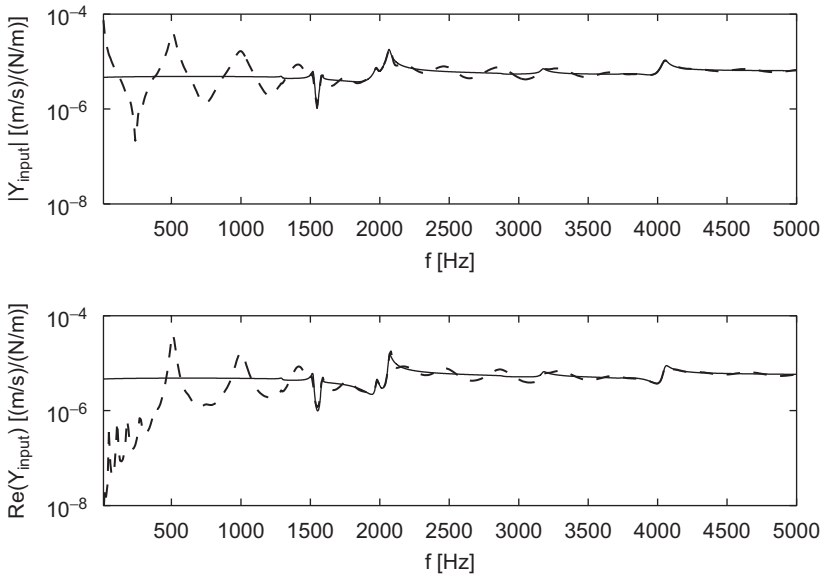

Fig. 21. Input mobility, profile strip A, $F_{1,x}$, (— infinite – – approximately infinite).

to form non-reflective ends. The end parts are both 2.5 m and with the loss factor η increasing gradually from 0.01 to 0.25.

The resulting wave amplitudes for all 12 waves (negative and positive going) are shown in Fig. 20 for strip A. The wave amplitudes for strips B and C are not shown for the sake of brevity. The calculation is done for

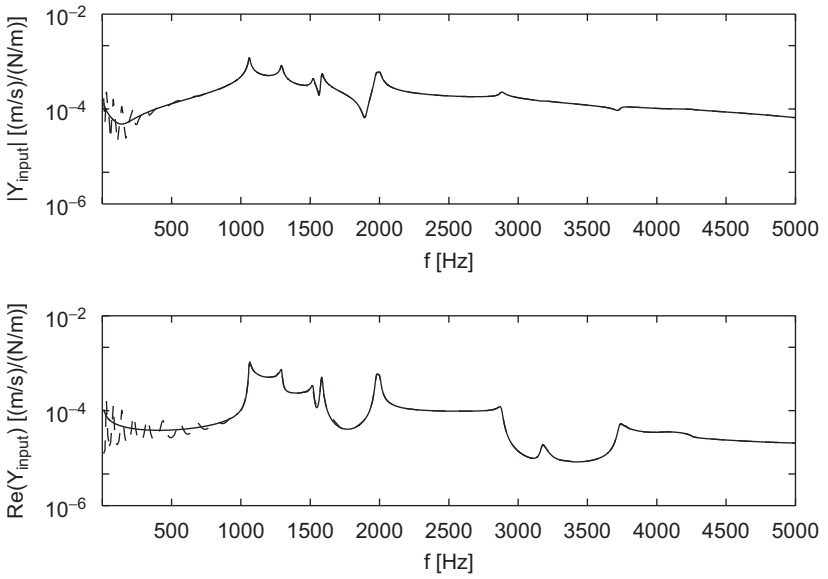

Fig. 22. Input mobility, profile strip A, $F_{1,y}$, (— infinite – – approximately infinite).

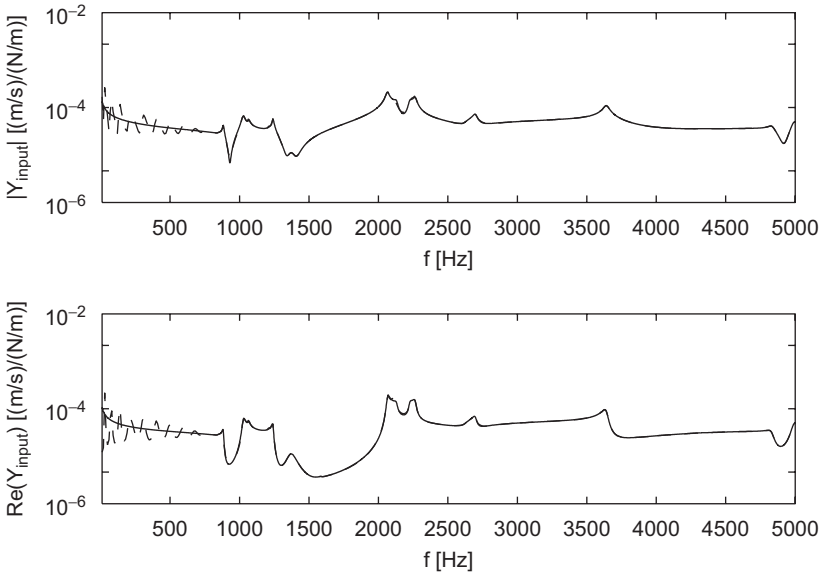

Fig. 23. Input mobility, profile strip B, $F_{1,y}$, (— infinite – – approximately infinite).

all three profiles and for two of the six excitation components ($F_{1,x}$; $F_{1,y}$). A selection of corresponding input mobilities is shown in Figs. 21–24. The $F_{1,x}$ excitation case is similar for all three strips and therefore only plotted for strip A.

The mobility for the infinite profile strips resemble those of the approximate, infinite strips at sufficiently high frequencies. Because of the longer wavelength for the longitudinal wave components, which are excited stronger by axial force excitation, the deviations are larger than for transversal force excitation.

The portion of the longitudinal waves is much higher in the low-frequency regime for axial excitation and all profiles than for transversal excitation. Because of the transition between the wave types this dominance is

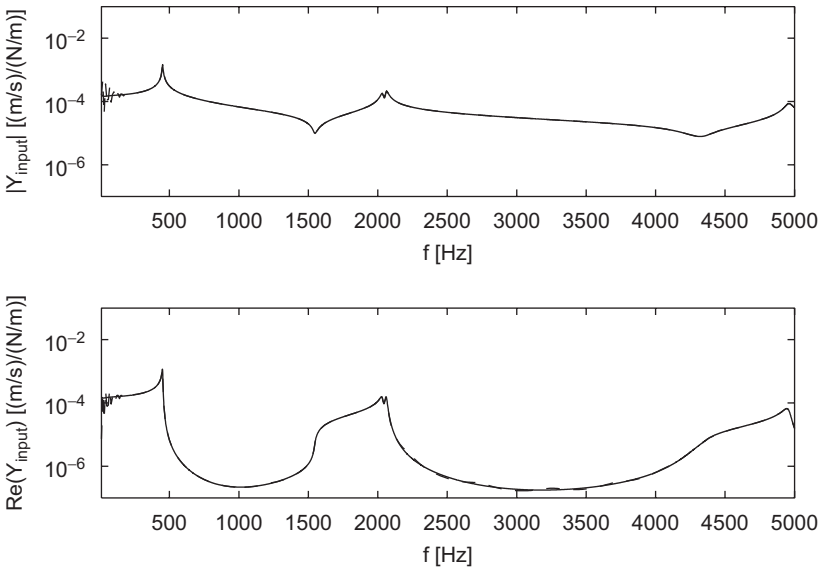

Fig. 24. Input mobility, profile strip C, $F_{1,y}$, (— infinite – – approximately infinite).

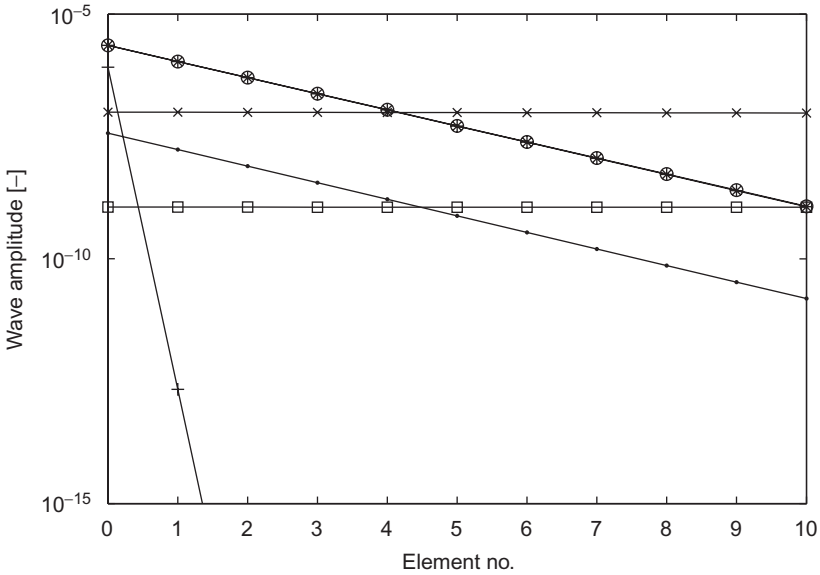

Fig. 25. Wave amplitudes of right-travelling waves along profile strip (Profile A) for force y-excitation at element number 0 (+ Wave 7, ○ Wave 8, ∗ Wave 9, • Wave 10, × Wave 11, □ Wave 12).

reduced at high frequencies. For the transversal excitation the 'bending' type waves are dominant in the pass bands.

It is anticipated that the wave amplitudes are changing along the profile, at least for decaying and complex waves. Wave amplitudes shown in Fig. 20 are given for the point of excitation. Two examples of the wave amplitudes along the strip are shown for profiles A and B in Figs. 25 and 26. Depending on the type of wave, the wave amplitudes decay strongly for complex and decaying waves and very little for propagating waves, where only the small structural damping attenuates the wave amplitudes.

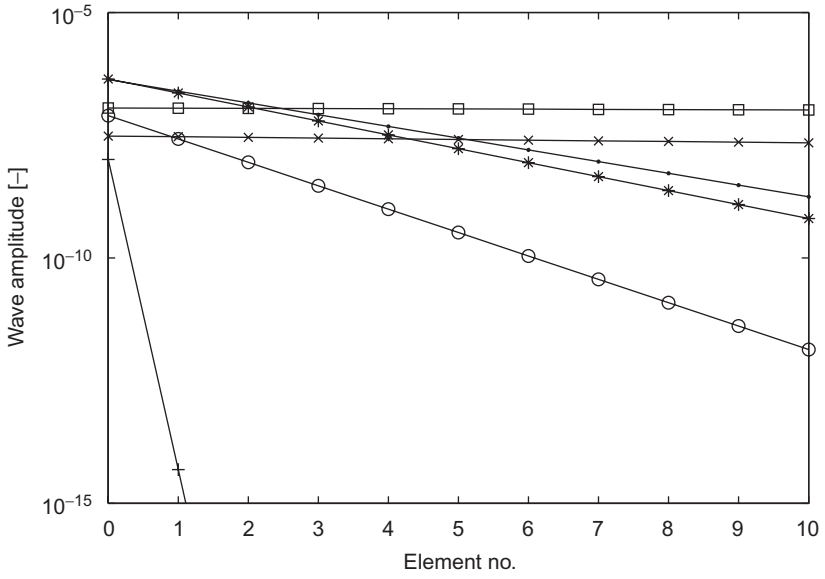

Fig. 26. Wave amplitudes of right-travelling waves along profile strip (Profile B) for force y-excitation at element number 0 (+ Wave 7, ○ Wave 8, ∗ Wave 9, • Wave 10, × Wave 11, □ Wave 12).

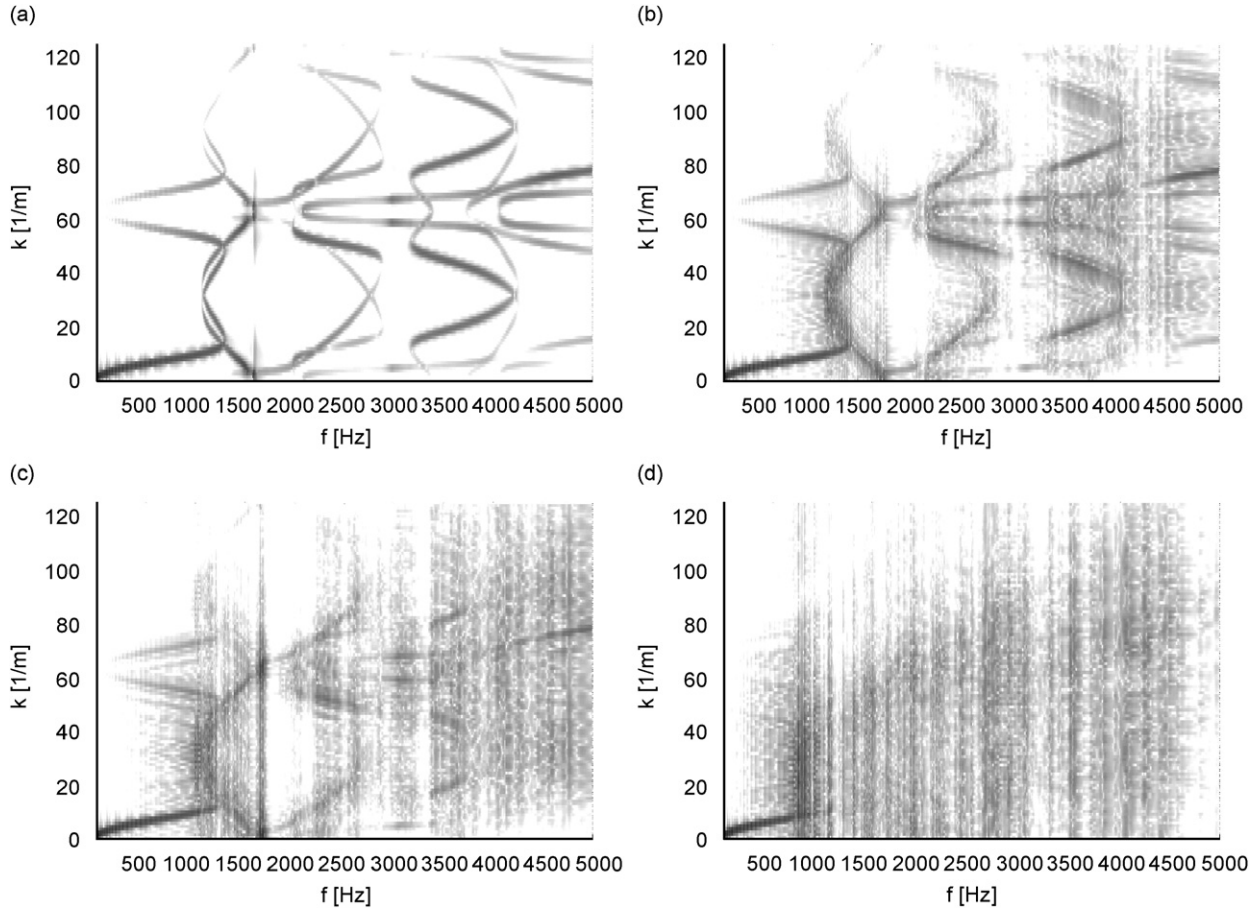

Fig. 27. Wavenumber plots using DFT of strip A introducing maximum random length variations of (a) 0%, (b) 5%, (c) 10% and (d) 50% (force excitation $F_{1,y}$).

6. Aperiodicity

6.1. Influence of periodicity perturbations on wave propagation

Apart from the DFT, the presented approaches for wavenumber extraction are only applicable to periodic profiles. However, as industrial profiles always have periodicity perturbations, it is of interest to investigate the influence of these perturbations on the dispersion characteristics. Different approaches are available:

- Application of the DFT method: the problem here is the low resolution if a short profile strip shall be investigated. One possibility to get a higher resolution is the use of a repeated strip. Moreover, the wavenumbers are smeared by the aperiodic features (see Fig. 27 for introducing random length variations to form aperiodic profiles based on profile A). For a randomization level of 5%, the characteristic wave distribution is conserved, for higher randomness, only the low-frequency behaviour is maintained whereas the high-frequency wavenumber components are smeared.
- Assuming that the periodic element is not part of the profile but is formed by the complete aperiodic profile, it should be possible to use the same tools as outlined for strictly periodic systems. In practice this would mean that one calculates the complete mobility matrix of the profile strip and uses the result in the determinantal equation to find the propagating waves. In the same way, the eigenvalue problem approach

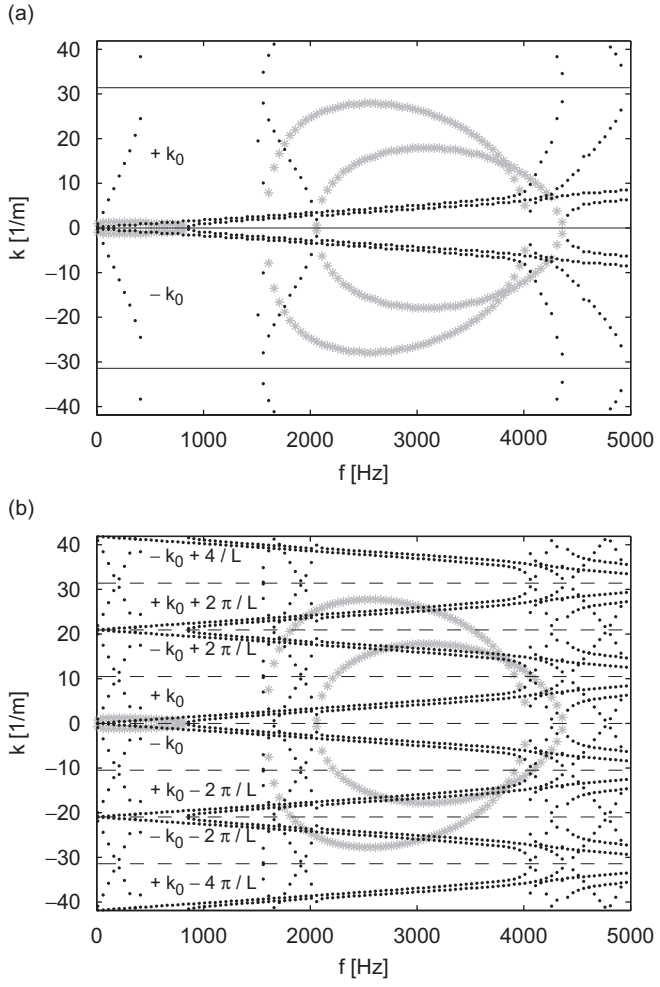

Fig. 28. Wavenumber plot extracted using determinantal equation based on (a) one element and (b) three elements for profile C (∗ (grey): decaying waves, ... (black) propagating waves).

using the T-matrix could be used. However, this is probably not practicable because of numerical instability of the transfer matrix for large systems.

The latter idea is marred by deficiencies. By using the mobility matrix of three coupled subelements the same wavenumber content can be extracted as for one subelement but additionally, there are other spurious waves coming into play. The periodicity of the wave number spectrum with period $2\pi/L_e$ introduces these additional spurious waves as L_e increases if more than one element is used. Due to this fact the results using the complete aperiodic strip will not give real insight in the wave propagation characteristics as the periodicity 'hides' the dominating wavenumbers.

Fig. 28 illustrates the resulting spectrum for three subsystems in comparison with only one subsystem. The additional wavenumbers in the plots can be linked to the original ones by mirroring the original values at the periodic lines $(\pi/L_e + n2\pi/L_e)$.

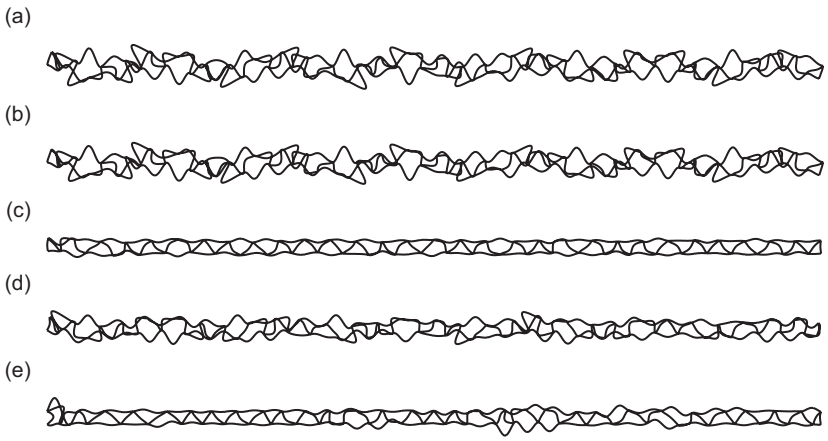

Fig. 29. Deflection shapes of (a) strictly periodic profile strip A, (b) maximum 1%, (c) 5%, (d) 10%, (e) 50% random length variation. Force excitation F_y at left end, 2500 Hz. Same scaling is maintained for all subplots.

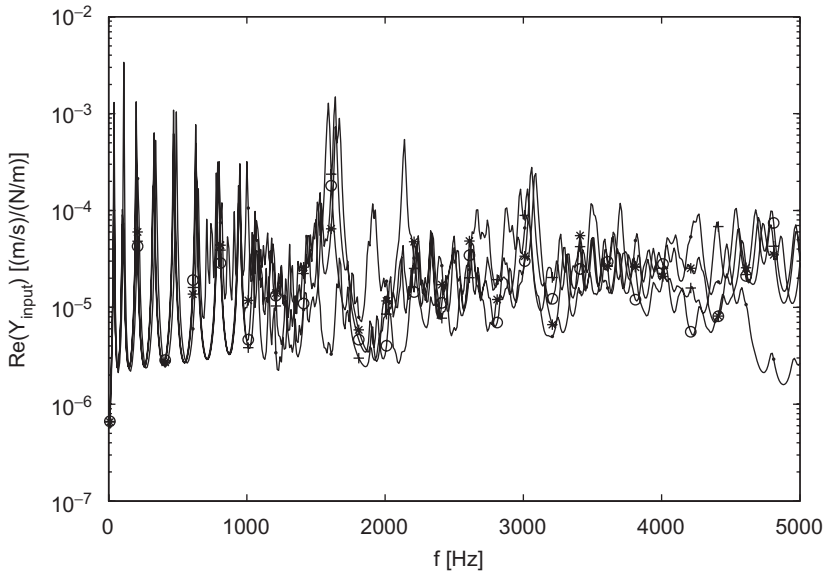

Fig. 30. Input mobility for randomly varied profile strip A (force excitation in y-direction at left end) + strictly periodic, ∘ 5%, ∗ 10%, • 50% random length variations of subsystems.

Upon solving the eigenvalue problem of the T-matrix the results, not included here for the sake of brevity, show the strong numerical instabilities arising. No meaningful results can be obtained for more than two elements.

In summary, only the DFT method is applicable for the extraction of wavenumber contents of aperiodic profile strips; the methods used for strictly periodic strips fail.

6.2. *Influence of periodicity perturbations on deflection shapes and mobilities*

One objective of this study is the determination of an acceptable criteria for the perturbations up to which the influence is of minor importance. Therefore, different calculations with the generic finite profiles presented in

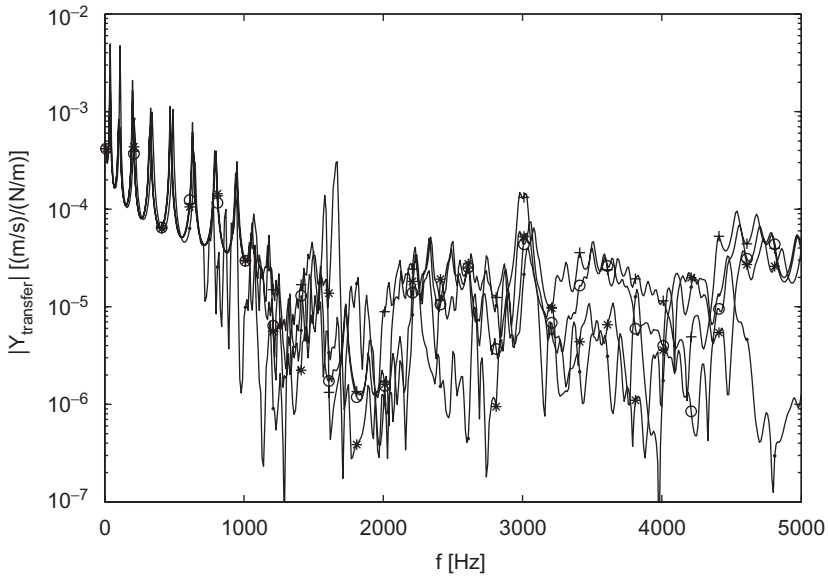

Fig. 31. Transfer mobility for randomly varied profile strip A (force excitation in y-direction at left end, response in y-direction approximately at centre of strip) + strictly periodic, ○ 5%, ∗ 10%, • 50% random length variations of subsystems.

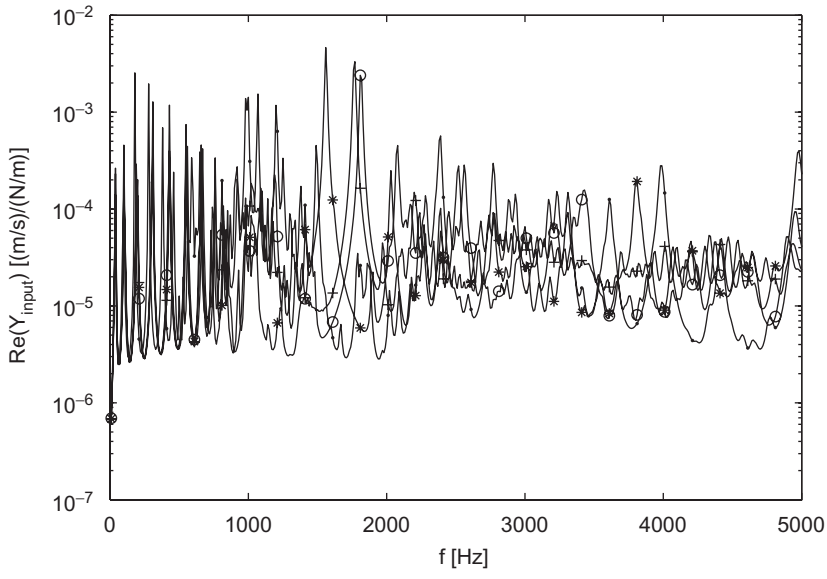

Fig. 32. Input mobility for randomly varied profile strip B (force excitation in y-direction at left end) + strictly periodic, ○ 5%, ∗ 10%, • 50% random length variations of subsystems.

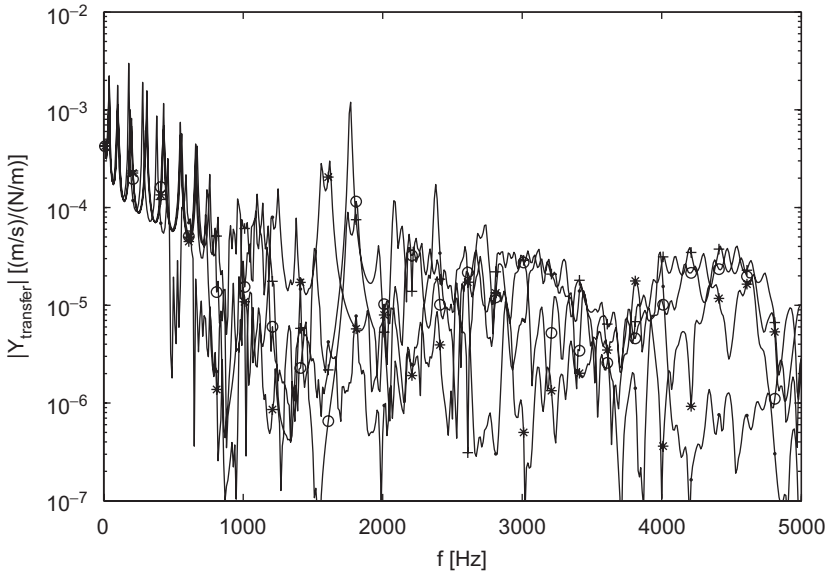

Fig. 33. Transfer mobility for randomly varied profile strip B (force excitation in y-direction at left end, response in y-direction approximately at centre of strip) + strictly periodic, ○ 5%, ∗ 10%, • 50% random length variations of subsystems.

Ref. [16] are performed with random perturbations. In this case, the length of each subsystem is varied with a uniformly distributed random number on an interval set by the maximum deviation (in percent) from the original periodic length. Values in the range from 1% to 50% are used and results for deflection shapes are shown in Fig. 29.

A more general investigation of this topic requires, e.g. Monte-Carlo simulations with different random deviations. This is not done in detail here because of the inherent computational and evaluation effort involved. Only one kind of randomization is considered. This can provide an informative basis for the influence of periodicity perturbations.

For profile A the forced deflection shapes (excitation F_y at left end) are shown in a pass band (2500 Hz) in Fig. 29. 1% randomness does not alter the deflection form, the 5% realization reduces the vibration levels on the complete strip significantly. For 50% random length variation the vibration is localized in some regions of the strip.

The influence on the input and transfer mobility is plotted for profile A in Figs. 30 and 31. The strip is force excited at the left end in the y-direction and the response is observed at a joint approximately at the centre of the finite strip, also in the y-direction. The corresponding plots for profile B are shown in Figs. 32 and 33 and for profile C in Figs. 34 and 35. As in Ref. [16] the results are again plotted for a force per unit length in z-direction. In order to increase legibility, the 1% variation case is suppressed. It is obvious that only large perturbations in the structure have significant influence on the mobilities. For profile C, where distinct pass and stop bands are present, the random length variations have only a small effect on the general trends. The influence on the transfer mobilities is more pronounced than for the real part of the input mobility. For the low-frequency behaviour, the influence of periodicity perturbations is less pronounced than for higher frequencies, where significant distortion of the pattern is more commonplace.

These results suggest that periodic effects will not disappear by small perturbations, at least for the investigated geometries. Hence, it seems viable to design structures in a way to use e.g. the stop band behaviour for noise control purposes.

7. Concluding remarks

The complete picture of propagating, decaying and complex waves can be gained by solving the transfer-matrix eigenvalue problem. For the profiles considered up to six characteristic waves can be identified, travelling in each direction. The wavenumber content in each characteristic wave is formed of several

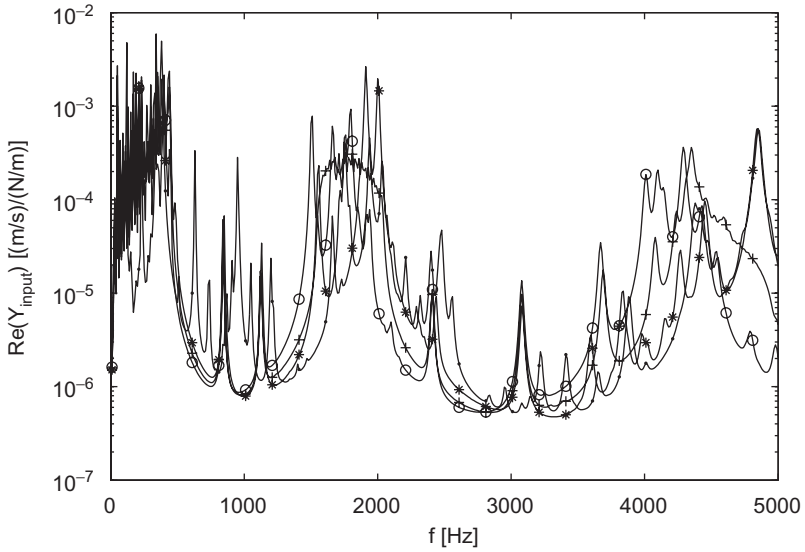

Fig. 34. Input mobility for randomly varied profile strip C (force excitation in y-direction at left end) + strictly periodic, ○ 5%, ∗ 10%, • 50% random length variations of subsystems.

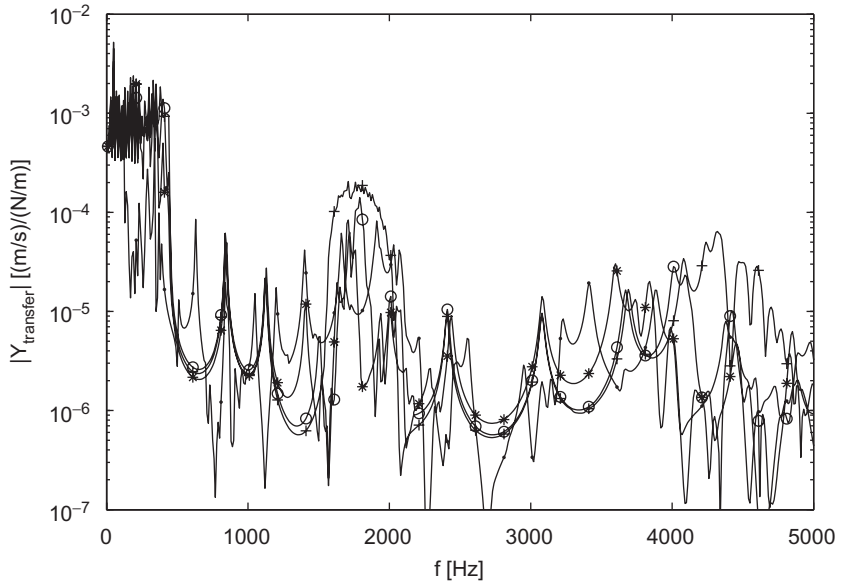

Fig. 35. Transfer mobility for randomly varied profile strip C (force excitation in y-direction at left end, response in y-direction approximately at centre of strip) + strictly periodic, ○ 5%, ∗ 10%, • 50% random length variations of subsystems.

"space harmonics", realising a periodic wavenumber spectrum. The relative contributions in the wavenumber series are fixed for each characteristic wave and can be identified from the complete characteristic wave forms. The extraction of the characteristic waves establishes means to simplify the wave propagation in the light weight profile strips. Provided there is a limited number of excitation points the decaying and complex waves will not contribute significantly to the overall vibration of the strip.

The amplitudes of the characteristic waves for forced vibrations of infinite profile strips and resulting mobilities can be calculated by using the dynamic stiffness matrix of a single periodic subsystem. The amplitudes

and the wavenumber content of each characteristic wave establishes the basis for a quantitative wavenumber distribution on the profile faces, which can be used for structure-borne sound and radiation problems.

A brief study on irregularity effects shows that the influence is limited. The general dynamic behaviour of the periodic profiles are conserved even for high random length variations of up to 10%.

References

[1] D.J. Mead, Wave propagation and natural modes in periodic systems: I. Mono-coupled systems, *Journal of Sound and Vibration* 40 (1) (1975) 1–18.

[2] D.J. Mead, Wave propagation and natural modes in periodic systems: II. Multi-coupled systems, with and without damping, *Journal of Sound and Vibration* 40 (1) (1975) 19–39.

[3] D.J. Mead, Wave propagation in continuous periodic structures: research contributions from Southhampton, 1964–1995, *Journal of Sound and Vibration* 190 (3) (1996) 495–524.

[4] T.S. Lok, Q.H. Cheng, Bending and forced vibration response of a clamped orthotropic thick plate and sandwich panel, *Journal of Sound and Vibration* 245 (1) (2001) 63–78.

[5] T.S. Lok, Q.H. Cheng, Free and forced vibration of simply supported, orthotropic sandwich panel, *Computers and Structures* 79 (2001) 301–312.

[6] P. Geissler, D. Neumann, Modeling extruded profiles for railway coaches using SEA, *Proceedings of the 1999 ASME Design Engineering Technical Conferences*, Las Vegas, Nevada, September 12–15, 1999.

[7] G. Xie, D.J. Thompson, C.J.C. Jones, A modelling approach for extruded plates, *Tenth International Congress on Sound and Vibration*, Stockholm, Sweden, number 882, 7–10 July, 2003.

[8] C. Pezerat, J.L. Guyader, Analytical modelling of extruded plates, *Proceedings of Euronoise*, Naples, 2003, pp. 1–6.

[9] R. Michael El-Raheb, Frequency response of a two-dimensional trusslike periodic panel, *Journal of the Acoustical Society of America* 101 (6) (1997) 3457–3465.

[10] J. Signorelli, A.H. Von Flotow, Wave propagation, power flow, and resonance in a truss beam, *Journal of Sound and Vibration* 126 (1) (1988) 127–144.

[11] E. Emaci, M.A.F. Azeez, A.F. Vakakis, Dynamics of trusses: numerical and experimental results, *Journal of Sound and Vibration* 214 (5) (1998) 953–964.

[12] M. Ruzzene, Vibration and sound radiation of sandwich beams with honeycomb truss core, *Journal of Sound and Vibration* 277 (2004) 741–763.

[13] L. Brillouin, *Wave Propagation in Periodic Structures*, McGraw-Hill, New York, 1946.

[14] B.A.T. Petersson, Influence of structural periodicity perturbations on transfer and cross transfer mobilities, TNO-Report TPD-HAG-RPT-950093, TNO Institute of Applied Physics, Delft, The Netherlands, May 1995.

[15] D.J. Mead, Free wave propagation in periodically supported infinite beams, *Journal of Sound and Vibration* 11 (2) (1970) 181–197.

[16] T. Kohrs, B.A.T. Petersson, Investigation of the two-dimensional wave propagation in typical light-weight profiles, in: M.J. Brennan (Ed.), *IX International Conference on Recent Advances in Structural Dynamics*, Institute of Sound and Vibration Research, University of Southampton, Southampton, UK, 2006.

[17] D.J. Mead, *Passive Vibration Control*, Wiley, New York, 1998.

[18] L. Friis, M. Ohlrich, Coupling of flexural and longitudinal wave motion in a periodic structure with asymmetrically arranged transverse beams, *Journal of the Acoustical Society of America* 118 (5) (2005) 3010–3020.

[19] R.C. Engels, Response of infinite periodic structures, *Journal of Sound and Vibration* 69 (2) (1980).

[20] D.J. Thompson, Wheel–rail noise generation, part III: rail vibration, *Journal of Sound and Vibration* 161 (3) (1993) 421–446.

[21] G.P. Brown, Determining the response of infinite, one-dimensional, non-uniform periodic structures by substructuring using waveshape coordinates, *Journal of Sound and Vibration* 287 (2005) 505–523.